LA-5372

Weapons Neutron Research Facility (WNRF) Storage Ring System--Technical Study

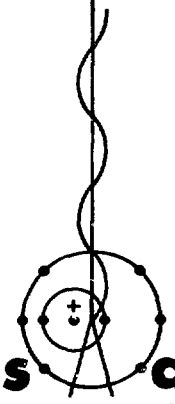

los alamos
scientific laboratory
of the University of California
LOS ALAMOS, NEW MEXICO 87544

UNITED STATES
ATOMIC ENERGY COMMISSION
CONTRACT W-7405-ENG. 36

Printed in the United States of America. Available from
National Technical Information Service
U. S. Department of Commerce
5285 Port Royal Road
Springfield, Virginia 22151
Price: Printed Copy $4.00; Microfiche $1.45

LA-5372
UC-28
ISSUED: December 1973

Weapons Neutron Research Facility (WNRF) Storage Ring System--Technical Study

Compiled by

Albert J. Lieber

CONTENTS

FOREWORD

It is virtually impossible to acknowledge properly all those who have been kind enough to contribute to this work. It is difficult to credit specific individuals for ideas because of the nature of the team effort and interactions of the parties working on the WNRF PSR. Some of the contributors, along with their areas of interest, are:

R. T. Avery, LBL (kicker channel and power supply, PSR fast quads)

R. K. Cooper, Hayward State College (theoretical section)

A. Garren, LBL (lattice geometry)

Jack Gunn, LBL (magnet engineering, vacuum system)

Klaus Halbach and Steve Magyary, LBL (pole-tip design)

P. F. Meads, Jr., Wm. M. Brobeck & Associates (lattice geometry, orbit analysis)

V. Kelvin Neil, Lawrence Livermore Laboratory (LLL) (theoretical section)

Carl E. Nielsen, Ohio State University (theoretical assistance and instrumentation)

LASL, Group P-11: Richard F. Bentley (chopper, buncher, kicker), John A. Farrell (beam transport optics), Thomas D. Hayward (ion source development and stripper calculations), and George P. Lawrence (ion source development, final editing)

The above parties, together with the author, fervently hope this work will serve to bring the WNRF PSR project to fruition.

WEAPONS NEUTRON RESEARCH FACILITY (WNRF) STORAGE RING SYSTEM--TECHNICAL STUDY

Compiled by

Albert J. Lieber

ABSTRACT

This report delineates the present engineering and theoretical design status of the Weapons Neutron Research Facility (WNRF) proton storage ring. It is the intent of this work to show that a practical set of concepts now exists for construction of this very desirable device for the WNRF. This storage ring will store 800-MeV protons from the Los Alamos Meson Physics Facility (LAMPF) to produce intense pulses for the subsequent generation of neutron pulses for direct weapon-mockup testing and studies related to the weapons program. Two basic modes of operation are planned to encompass the scope of experimental investigations. The first mode will consist of loading the ring to attain the greatest unbunched (dc) circulating current that can be contained (a goal for this operation is 100 A) and the release of this current in one pulse of approximately 200-nsec duration. This mode will be used for weapons-related studies that require very intense pulses. The second mode will consist of the accumulation of five 5-nsec-wide bunches of protons circulating in the storage ring, and the subsequent release of these bunches to form a pulse train at the rate of 600 pps on a continuous basis. This mode will be used for weapons-related measurements involving high resolution time-of-flight energy analysis of neutrons. Charge-exchange injection will be employed in both modes of operation because of the demonstrated brightness advantage over conventional synchrotron or betatron space stacking.

I. INTRODUCTION

A. Background

Intensive research in storage ring development began in 1956 when Kerst et al. and Brobeck independently suggested that such devices would be useful in high-energy research as a means of increasing the reaction energy in the center-of-mass coordinate system and the reaction probability.[1,2] The energy in the center-of-mass system could be increased by head-on collisions of identical relativistic beams, and the reaction probability increased by recirculation of these beams through the reaction channel. O'Neill proposed that the synchrotron could be used as an injector for intersecting storage rings.[3] These studies have culminated in the construction of the CERN Intersecting Storage Ring (ISR), SPEAR, and the storage rings at Novosibirsk, USSR.[4-6] Traditionally, a variation of the concept became popular in low-energy and medium-energy nuclear physics as a means of transforming accelerator duty factors. Existing cyclotrons, especially frequency-modulated machines, had such low duty factors that investigations of important low cross-section reactions were hampered by detector pile-up. This led to the discovery that the cyclotron could be used to accelerate particles to near the extraction radius, where they were stored, and another electrode system used to manipulate the duty factor through slow spill or dribble extraction during each cycle. This concept was first used at the Lawrence Berkeley Laboratory (LBL) 184-in. machine and later copied at smaller machines involved in low-energy cross-section work.[7,8]

The above work is noted because the requirement for beam manipulation in the Weapons Neutron Research Facility (WNRF) is opposite to general usage. A proton storage ring (PSR) will be used to compress or shorten the duty factor of the Los Alamos Meson

Physics Facility (LAMPF) and thereby increase the neutron pulse capability of the Laboratory. This will be accomplished by the injection and accumulation of the LAMPF beam, followed by a programmed fast ejection of all or part of the stored protons into the WNRF transport system, leading to a neutron-producing target. Although increasing the duty factor of LAMPF to 100% can also be accomplished by the PSR using continuous injection and slow spill extraction, the main character of neutron investigations requires intense packets of particles to serve as input functions for time-of-flight weapons investigations. The addition of the PSR to WNRF will yield an unmatched pulse capability and thereby open whole new horizons of experimental measurements related to the Laboratory's programmatic weapons studies.[9] The importance of these measurements as a supplement to field testing cannot be overemphasized.

B. Summary of Storage Ring Development and Operation

Recent advances in the technology and utilization of negative hydrogen ion sources have had a dramatic impact on the WNRF PSR program. These advances will make it possible to construct a more versatile and simpler machine than outlined previously,[10] with containment performance based upon solid experimental precedent. For these reasons, and in order to reduce the lead time to utilization of the full PSR potential, the program has been divided into two phases. Phase I (PSR I) will consist of the construction of the experimental storage ring in a properly shielded building located next to the WNRF beam transport line without the allied experimental buildings necessary to use the full pulse potential of the ring for long periods. Location of this building relative to WNRF is shown in Fig. 1. The WNRF portion of the LAMPF switchyard has been designed to transport the negative hydrogen ion beam to the ring on a sole-use basis for PSR I; thus, the beam will probably be delivered only occasionally for storage ring testing and operation for specific weapon-programmatic measurements. The transport line will also transport protons to WNRF for regular laboratory operation. The present design of the WNRF portion of the LAMPF switchyard is such that, with a minimum of modification, the negative hydrogen beam could be time-shared with other experimental areas in Phase II (PSR II) operation if it is economically desirable. For PSR II operation, in addition to specialized experimental area construction and LAMPF switchyard modifications, the PSR would be redesigned and modified to withstand the steady, high-radiation environment. A separate proposal will be prepared for PSR II when feasibility measurements of PSR I warrant it.

Two operational modes are planned for the PSR to encompass the wide spectrum of experiments planned for WNRF. The first, designated the pulse mode, will provide a continuous series of extracted pulses of 5-nsec width at a repetition rate of 600 pulses/sec. This mode will be useful to that generic type of experiment employing neutron time-of-flight energy analysis. The second mode of operation, which we shall designate here as the high-current mode, will consist of loading the PSR in such a manner as to obtain the maximum unbunched (dc) current of protons, followed by single-turn extraction of these particles, thus providing a very intense pulse of approximately 200-nsec duration. This mode will be of primary use in weapons diagnostics.

The procedure of following a beam particle from injection to the PSR target may be useful in understanding the ring system operation. The LAMPF negative hydrogen ion beam will be used for both modes of storage operation, thereby simplifying the beam handling and injection system. The H^- beam will, after generation and transport to the PSR, be stripped to form neutral hydrogen atoms (H^0) outside

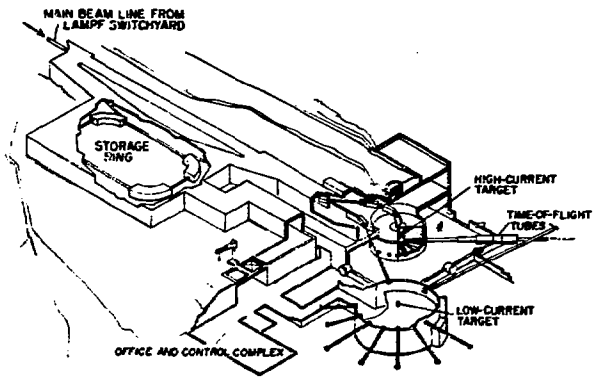

Fig. 1. Layout of the WNRF

the PSR magnet lattice. This neutral beam will be drifted across the magnetic field lines and stripped to form protons (H^+ ions) on the equilibrium orbit of the PSR. Use of negative hydrogen charge-exchange injection for both modes of operation is attractive for several reasons. It was reported recently[11] that this technique gives 100 times more brightness in the Argonne National Laboratory (ANL) booster storage ring than would have been achievable with conventional H^+ injection methods, and there is no apparent limitation on current storage using this method in the WNRF/PSR. That is to say, by using charge-exchange injection, the Liouville constraint on phase-space density, which is so troublesome in conventional synchrotron or betatron space storage of protons, can be effectively circumvented.[12] This is of utmost importance to WNRF because of the need for high beam brightness in both modes.

Neutron output performance specifications for WNRF/PSR are given in Table I, which shows several LAMPF input options, depending upon ion-source capability.

Circulation period for the ring has been chosen to be 248.5 nsec, which gives a circulation frequency exactly 2% of the 201.25-MHz LAMPF bunching frequency. Thus, for the pulse mode of PSR operation, the microstructure of beam injected into the PSR can be preserved, and synchronously added to, by using a single, simple 201.25-MHz bunching cavity slaved to the LAMPF master oscillator. In this mode, five bunches of protons will circulate 50 μsec apart in the PSR. Since the normal LAMPF microstructure consists of pulses 0.25 nsec wide and 5 nsec apart, a system of either bunching or chopping the LAMPF beam must be employed to add to the bunches circulating in the ring. Fortunately, both techniques will be available to us. First, negative ion sources will soon be available with emittance quality and current output capable of utilizing the full LAMPF potential for acceleration of a 17-mA negative hydrogen ion beam.[13] If such an ion source were employed, the beam could be chopped in the 750-MeV injector transport line by the WNRF chopper (which will be capable of single micropulse selection). The chopper would transmit every tenth pulse, which would then add in phase to the bunches circulating in the ring to yield a 3.4-A peak pulse current for 200 turn loading. This represents 50 μsec of the LAMPF macropulse. Another alternative is to capitalize on the discovery that it is possible to prebunch in the negative ion source itself.[14] If a modified 1.7-mA H^- source employed a 10X prebunching factor and released every tenth micropulse, it would produce equivalent pulse-mode bunches in the PSR of 3.4-A peak current, again with 200-turn injection. Finally, assuming no modification to the present LAMPF H^- ion source, a 3.4-A peak pulse could be obtained by chopping the LAMPF injected beam of 1.7 mA and loading the PSR for 2000 turns (one full macropulse of LAMPF).

The beam transport line from LAMPF to the PSR has been so designed that no LAMPF modifications are required for it to carry the H^- beam without time-sharing. All bending magnets have been designed to operate at low fields (of the order of 4 kG) to minimize the motional electric-field stripping of the weakly bound electron of the H^- ion. The transfer line to the PSR consists of an achromatic translation of 25-ft displacement from the main WNRF beam channel (Fig. 1). This system is made up of two 6.8° bending magnets at each end of the translation and five quadrupole lenses located between the bends. There is a matching quadrupole doublet between the last 6.8° magnet and the PSR. TRANSPORT code calculations show this arrangement to be sufficient to match the beam to the betatron functions of the PSR and to yield point-to-point imaging from the LAMPF switchyard kicker magnet to the match point at the PSR.[15] This system minimizes jitter problems in the transport system caused by power supply ripple. The injection transport line to the PSR is composed of standard bending magnets and quadrupoles used elsewhere in WNRF. Approximately 4 m of clear space are available between the last quadrupole doublet and the PSR for location of the H^- to H° stripper system.

There are several ways to achieve the H^- to H° transition before the H° atoms drift across field lines into the PSR, and a machine development experiment is scheduled at LAMPF to determine the optimum method.[16] One attractive method would be to use a coaxial helical xenon flash lamp similar in design to that used for laser pumping to photodetach the weakly bound electron. Another method would be to use a large magnetic field step to detach the electron by motional electric-field stripping.

TABLE I

WNRF/PSR NEUTRON SOURCE CHARACTERISTICS

Program Phase/Mode	LAMPF Beam Requirements: Beam	Pulse Rate	Pulse Length	Time Sharing	Chopper Operation	PSR Storage Conditions	WNRF Neutron Capability: Neutrons/[a] Pulse	Pulse Length	Pulse Rate
WNRF	17 mA H^+	120 pps	2→7 μsec	Yes	Preparation of WNRF pulse and blanking for kicker magnet	No storage	Single Micropulse: 1.1×10^{10}	1 nsec	120 pps
							Up to 5-μsec of Macropulse: $\leq 1.1 \times 10^{13}$	≤5 μsec	120 pps
PSR I/Pulse	1.7 mA H^-	120 pps	500 μsec	No	Transmit every tenth micropulse/50-nsec intervals	2000 turns, 5 bunches circulating, 10^{11} protons each, 3.4-A peak pulse current	2.0×10^{12}	5 nsec	600 pps
PSR 1/Pulse	1.7 mA H^-	120 pps	50 μsec	Partial[b]	Prebunching in ion source for X10 enhancement every tenth micropulse	200 turns,[c] 5 bunches circulating, 10^{11} protons each, 3.4 A peak pulse current	2.0×10^{12}	5 nsec	600 pps
PSR I/Pulse	17 mA H^-	120 pps	50 μsec	Partial	Transmit every tenth micropulse/50-nsec intervals	Same as above	2.0×10^{12}	5 nsec	600 pps
PSR I/ High Current	1.7 mA H^-	Occasional	500 μsec	No	Off	6000 turns, 3 consecutive macropulses, 10-A average current	2.5×10^{14}	200 nsec	Occasional
PSR I/ High Current	17 mA H^-	Occasional	500 μsec	No	Off	2000 turns, 1 macropulse, 34-A average current	8.4×10^{14}	200 nsec	Occasional
PSR II/Pulse	Same as in PSR I, above, except that time sharing of H^- in the conventional manner (with line X) is allowed.								
PSR II/ High Current	17 mA H^-	Occasional	500 μsec	No	Off	2000 turns, 1 macropulse, 34-A average current	8.4×10^{14}	200 nsec	Occasional
PSR II/ High Current	17 mA H^-	Occasional	500 μsec	No	Off	Goal to store 3 macropulses, 100 A average current	2.5×10^{15}	200 nsec	Occasional

[a] Based on assumption of 20 neutrons produced per incident proton by WNRF target.

[b] Remainder of H^- macropulse could be used in Area A; positive beam in Area B or C if desired.

[c] Much larger peak pulse stored currents may be achievable by injecting a longer portion of the macropulse, subject to the limitation imposed by beam instabilities.

The H° beam will be introduced into a magnetic lattice of racetrack configuration having overall dimensions of 9.9 m by 21.2 m. Basic magnets for the 90° bends will be the ¼-scale Bevatron magnets, brought to LASL for this purpose. Use of these magnets should result in a cost saving, and their wide apertures can be adapted to this application by the addition of alternating-gradient pole tips and correction coils. The vacuum vessel for the PSR will be of stainless steel and will employ distributed ion pumps operating in the main alternating-gradient magnet. This system will allow the potential of achieving ultrahigh vacuum (UHV), which will provide a margin of safety should problems in high-beam stability be encountered later in the storage ring development.

Extraction of the circulating beam of protons in the PSR will be accomplished by deflecting the beam 12.5 mr upward into a septum magnet. A fast kicker magnet located between a 90° bending magnet and the next quadrupole in sequence will be used for this initial deflection. The action of this quadrupole and the following two quadrupoles yields an upward displacement of 3.4 cm at the entrance to the septum leading to the WNRF transport line.

The septum magnet bends the beam 8.7° horizontally. Following the septum, a second 8.7° bend brings the total deflection angle to 17.4°. These magnets can operate at 15-kG fields because the ejected particles are now protons. TRANSPORT calculations predict that a 1.5-cm-diam spot can be achieved at the WNRF target, assuming horizontal and vertical stored beam emittances in the ring of 2π cm-mr and a momentum spread ($\Delta p/p$) of ±0.25%. The present limiting factor on spot size is the dispersion produced by the 30° bending magnet that switches the beam to the target room. Should a very small spot be desired at a later date, the system can be made achromatic with additional quadrupoles. A summary of the PSR operating parameters is given in Table II.

II. MACHINE DESIGN

A. Magnet Lattice

1. Configuration. The circumference of the PSR is constrained by the desire to limit the time duration of the (single-turn) extracted beam to about 200 nsec. The layout is also constrained by the high cost per square foot of the building to house the PSR because of the heavy shielding requirement. If there is to be adequate straight-section length for beam extraction within this limited circumference, the ring must have a minimum number of very long straight sections connecting a tight alternating-gradient lattice in the curved portion of the PSR.

Compact bending arrays can be achieved either with a separated-function magnet structure with zero-gradient bending fields of approximately 20 kG or with combined-function magnets with a guide field of approximately 14 kG. Such high guide fields are acceptable in the PSR because the protons are not accelerated, whereas they would not be acceptable in a fast-cycling synchrotron because of stored-energy considerations in the changing fields.[17] Ideally, drift lengths in the bending magnet should be minimized, providing only enough room for coil terminations, vacuum fittings, etc. An optimum bending array would consist of continuous bends of 90 or 180° with no included drift lengths but with an adequate focusing structure. For this purpose, combined-function magnets are superior to separated-function magnets.

With the choice of at least two long drift sections to minimize floor area, very long drift spaces are possible within the limits of the previously discussed circumference boundary condition. A new type of insert will be used to provide long drift lengths, as well as perfect linear matching in both planes, including the equilibrium orbit for protons differing in momentum from the design momentum. This is the π-2π "invisible straight section" which has been described in the literature.[18]

The resultant racetrack geometry for the PSR, based on the aforementioned boundary conditions, is shown in Fig. 2. With the π-2π insert, it is best to use a symmetrical bending array (FOFDOD*), and this geometry was chosen for the PSR. Shortly thereafter we learned of the imminent decommissioning of the California Institute of Technology's (CIT) electron synchrotron. Because its magnet (which was once the quarter-scale model of the Bevatron) was designed for particles of magnetic rigidity comparable to the 800-MeV protons to be stored in the PSR,

*F = (radial) focusing section, D = (radial) defocusing section, O = drift section.

TABLE II

WNRF PSR PARAMETERS

Kinematic Parameters of Stored Protons			
Kinetic energy	E	800	MeV
Relative velocity	$\beta = v/c$	0.841821	
Relative mass	$\gamma = (1-\beta^2)^{-1/2}$	1.852688	
Relative momentum	$\beta\gamma$	1.559632	
Momentum	$p = \beta\gamma mc$	1.463264	GeV/c
Magnetic rigidity	$B\rho$	48.809234	kG-m
Physical Characteristics of PSR			
Nominal magnetic guide field	B_o	12.9839	kG
Orbit period	τ	248.447	nsec
Circumference	C	62.7010	m
Average radius	$R = C/2\pi$	9.97918	m
Magnetic radius	ρ	3.75930	m
Number of long straight sections	N	2	
Length of superperiod	C/N	31.3505	m
Number of normal periods	n	4	
Structure of normal periods	OFDDFFDDFO		
Length of normal period	L	7.80696	m
Average radius of normal period		4.97006	m
Length of drift space	L_0	0.950932	m
Length of F magnet	L_F	1.7715	m
Length of D magnet	L_D	1.1810	m
Magnetic field profile of F magnet	k_F	3.2000	m^{-1}
Magnetic field profile of D magnet	k_D	-4.0000	m^{-1}
Available apertures within gradient magnets			
radial		15.8	cm
vertical		5.4	cm
Insertion			
type of insertion		π-2π long straight section	
length of insertion	L_i	15.7366	m
length of unobstructed central drift space	L_c	7.0000	m
length of end drift spaces	L_e	0.9870	m
length of drift space between Q1 and Q2	L_{12}	2.0302	m
length of drift space between Q2 and Q3 (measured from quadrupole effective ends)	L_{23}	0.4367	m
effective length of quadrupole magnets	L_Q	0.3048	m
gradients of quadrupole magnets in insertion			
first and last quadrupoles	B'_1	0.94168	kG/cm
second and fifth quadrupoles	B'_2	-1.51915	kG/cm
third and fourth quadrupoles	B'_3	1.51424	kG/cm
maximum pole-tip field in quadrupoles	B_{max}	10.00	kG
full aperture of quadrupole magnets	a	13.17	cm
Orbit Parameters			
Number of betatron oscillations per revolution			
radial	ν_x	4.3637	
vertical	ν_y	2.3431	

(Table II, cont.)

Phase advance per normal period [OFDDFFDDFO]			
radial	μ_x	213	deg
vertical	μ_y	124	deg
Phase advance per long straight section			
radial	μ_{xs}	360	deg
vertical	μ_{ys}	180	deg
Mean betatron wavelength			
radial	λ_x	14.3688	m
vertical	λ_y	26.7597	m
Amplitude function β			
gradient magnets			
radial			
maximum		5.501	m
minimum		0.958	m
vertical			
maximum		9.659	m
minimum		1.829	m
long straight section			
radial			
maximum		7.630	m
minimum		0.576	m
vertical			
maximum		23.22	m
minimum		1.836	m
Momentum-compaction function η			
gradient magnets			
maximum		1.072	m
minimum		0.643	m
long straight section			
maximum		1.072	m
minimum		0.000	m
Transition energy	γ_t	3.392	
Momentum compaction function	$\delta = \gamma_t^{-2}$	0.08692	
Injector Characteristics [LAMPF H^- Beam]			
Long-term average, current		100[a]	μA
Macro duty factor		6	%
Macropulse repetition rate		120	pps
Duration of macropulse	τ'	500	μsec
Average beam current during macropulse		1.7[a]	mA
Number of H^- ions in macropulse		5.3×10^{12}[a]	
Structure of macropulse			
micropulse bunching frequency	f	201.25	MHz
micropulse interval	τ''	4.97	nsec
number of micropulses in macropulse		10^5	
number of H^- ions per micropulse		5.3×10^7[a]	
width of micropulse		0.25	nsec
instantaneous current in micropulse	i_{peak}	34[a]	mA
micropulse width entering storage ring		0.4	nsec

[a]Numbers refer to design performance of existing H^- ion source. Recent progress indicates that a much higher current (17 mA) H^- ion source can be constructed.

(Table II, cont.)

Relative momentum spread (recent measurements suggest that the actual spread may be much smaller than this value)	$\delta p/p_{max}$	±0.2	%
Emittance--radial and vertical planes (at 800 MeV) (recent measurements suggest that the actual emittance may be only 5% of this value)	ε	π	cm-mr
PSR radio-frequency accelerating system			
With 20.125-MHz H⁻ bunching in ion source, or 1 in 10 pulse selection in 750-keV line			
frequency		201.25	MHz
peak accelerating voltage per turn		100	kV
relative frequency modulation required (provided to enable beam to move away from stripper for situation where entire charge cannot be loaded in 1 macropulse)		4	%
Without bunching in source or chopping at 750 keV	Frequency		Voltage
beam homogenizing	805	MHz	538 kV
beam homogenizing	201.25	MHz	19% kV
pulse-mode bunching	20.125	MHz	14 kV
pulse-mode bunching	80.5	MHz	130 kV
relative frequency modulation required	≠ 201.25 MHz	4	%
Experimental requirements on beam			
Pulse mode			
number of bunches		5	
bunching factor		10	
bunch duration		5	nsec
number of protons in bunch		1.0×10^{11}	
number of protons in ring		0.5×10^{12}	
peak current	I_{max}	3.4	A
number of turns injected[b]		200/2000	
injection time[b]		50/500	μsec
High-current mode			
immediate objective (using 17-mA H⁻ source)		54	A
number of turns injected		2012	
injection time		500	μsec
number of protons extracted (assumes 50 nsec of 250-nsec pulse lost in beam spill)		4.35×10^{13}	
design current goal		100	A
number of protons extracted		1.25×10^{14}	
Chromaticity			
Without sextupole correction			
$\partial\nu/\partial(\delta p/p)$			
radial		-2.95	
vertical		-5.89	
Sextupole correction			
F magnets	$(\partial^2 B/\partial r^2)/B_o$	5.188	$/m^2$
D magnets		-10.147	$/m^2$
Trim coils			
sextupole gradient		eliminate or double the above increase or decrease by 5%	

[b] Depends on H⁻ injection option selected (see Table I).

we began an investigation of its use with new strong focusing pole tips. This magnet would provide a very nearly optimum bending array, while providing a desirably large aperture. A cost analysis by Jack Gunn, LBL, shows that use of these magnets for PSR I would result in a saving to the project of approximately $0.5 million.[19] Since these magnets are about 58% efficient, and a modern design would be about 85% efficient, the power loss penalty over a modern design has been estimated at $10,500 per year.

Cell structures of symmetrical and antisymmetrical types, adapted to the CIT quadrants, were studied. Minimum betatron and synchrotron amplitudes were obtained with an FODF type of lattice, covering an angular extent of 45°. With the "F" pole tip covering an angular extent of 13.5° and the "D" pole tip covering an extent of 9°, the interface between adjacent pole tips coincides with the existing breaks in the CIT magnet laminations. This would provide easy access to trim coil terminations--a desirable feature because of the complex geometry involved in dressing leads in the pole-face correction system to minimize interaction of the windings. Optimum magnetic field profiles ($k = \beta'/\beta_0$) for this structure are 3-4 m^{-1}. Therefore, in addition to the consideration of reusage, the CIT magnets appeared to be ideally suited for PSR I and they were brought to LASL for this purpose. A section through the magnet showing the strong focusing pole tips is shown in Fig. 3. The lattice was modified to a 90° cell of structure QFDDFFDDFQ, at the suggestion of A. Garren, to provide adequate separation of the coil ends without requiring additional matching sections.

The π-2π insert is symmetrical in its normal permutation and provides for minimum apertures when inserted at the F-F symmetry point in a FOFDOD type of lattice. For fixed quadrupole lengths and fixed insertion lengths, two free parameters are available for optimal fitting. These parameters are most conveniently chosen to be: (1) the length of the unobstructed central drift space (L_c) and (2) the radial magnification at the center of the insert relative to the end points (m). The vertical characteristics are nearly independent of these parameters and are thus not available for fitting. A complete study of the resultant geometries relative to PSR has been published.[20]

At the center of the insert, the 3X3 radial and 2X2 vertical transfer matrices, relative to either end point, are:

$$\begin{bmatrix} -m & 0 & 0 \\ 0 & -1/m & 0 \\ 0 & 0 & 1 \end{bmatrix} \text{[radial]} \quad \text{and} \quad \begin{bmatrix} 0 & f \\ -1/f & 0 \end{bmatrix} \text{[vertical]}$$

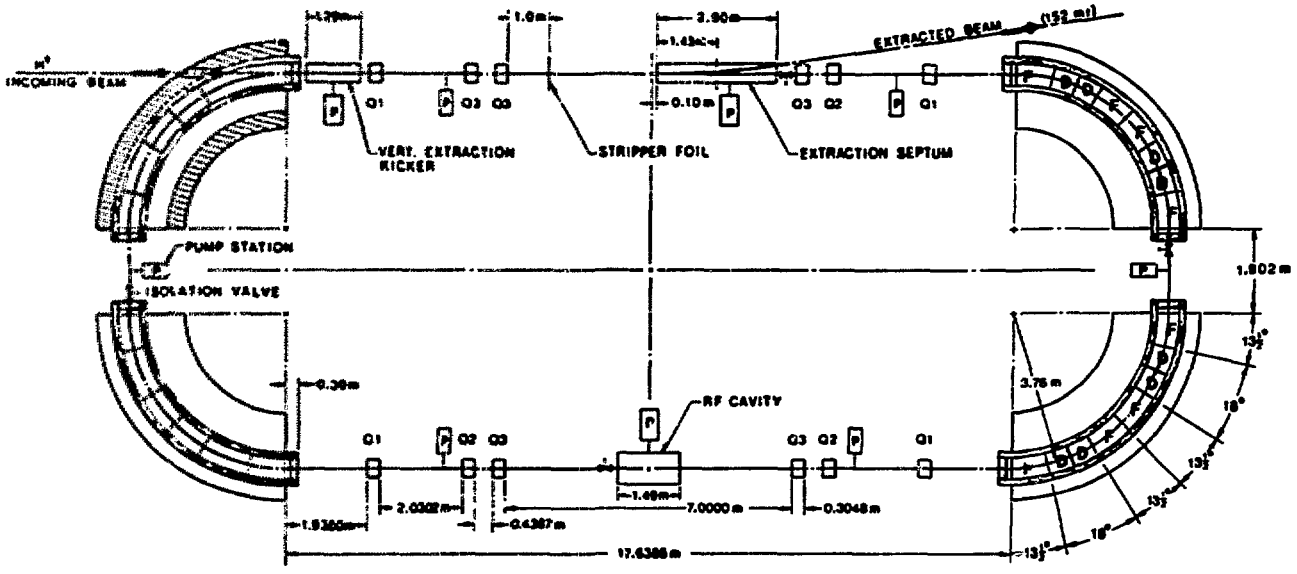

Fig. 2. WNRF storage ring.

As mentioned above, a desirable PSR circumference is such that the circulation frequency for 800-MeV protons is exactly 2% of the 201.25-MHz bunching frequency of LAMPF. The bunch microstructure can then be injected into the PSR to be maintained by a simple radio-frequency (rf) cavity slaved to the LAMPF master oscillator, a desirable arrangement for pulse-mode operation. For an insert of 15.74 m, which provides the proper circumference, the vertical midpoint focal length (f) lies between 2.5 and 3.0 m for all reasonable values of the free parameters.

If β_o and β_c are the amplitude functions at the end points and the center of the insert, respectively, in the radial plane, then $\beta_c = m^2\beta_o$. For the FOFDOD-type lattice provided by the CIT magnet structure, the radial β function at the F-F point lies between 5 and 8 m--depending on the magnetic field gradients. The radial beam width is maximum at the quadrupoles nearest the center of the insert.

For a central drift length of L_c, the maximum β is thus $\bar{\beta} = \beta_c + L_c^2/(4\beta_c)$. The minimum aperture is obtained when $\beta_c = L_c/2$. In terms of the β function at the end points, the minimum aperture condition is: $m^2\beta_o = L_c/2$. For extreme choices of parameters--those that maximize L_c, subject to being feasible--the end drift lengths are very small, and the optimal apertures are obtained for $\beta_o = \bar{\beta} = L_c = 2\beta_c$ which sets $m^2 = \frac{1}{2}$ and L_c between 5 and 8 m. These optimal conditions represent stationary values of the aperture, and significant departures from them will not significantly increase the aperture.

In the case of the PSR lattice, the insert is used primarily for extraction. Because of the large radial aperture, extraction is most economically obtained by providing the initial deflection in the vertical plane, with secondary deflection in the radial plane provided by an iron-septum magnet which does not interfere with the normal PSR aperture. This choice allows full unobstructed radial aperture usage without penalty. For example, this aperture allows the PSR to operate at an integral subharmonic of the 201.5 MHz for many proton energies by merely altering the guide field in the bending array. That is, it will be possible to alter the ring period to accommodate protons of other than 800-MeV energy or to prevent excessive longitudinal charge density during operation in the high-current mode. Should

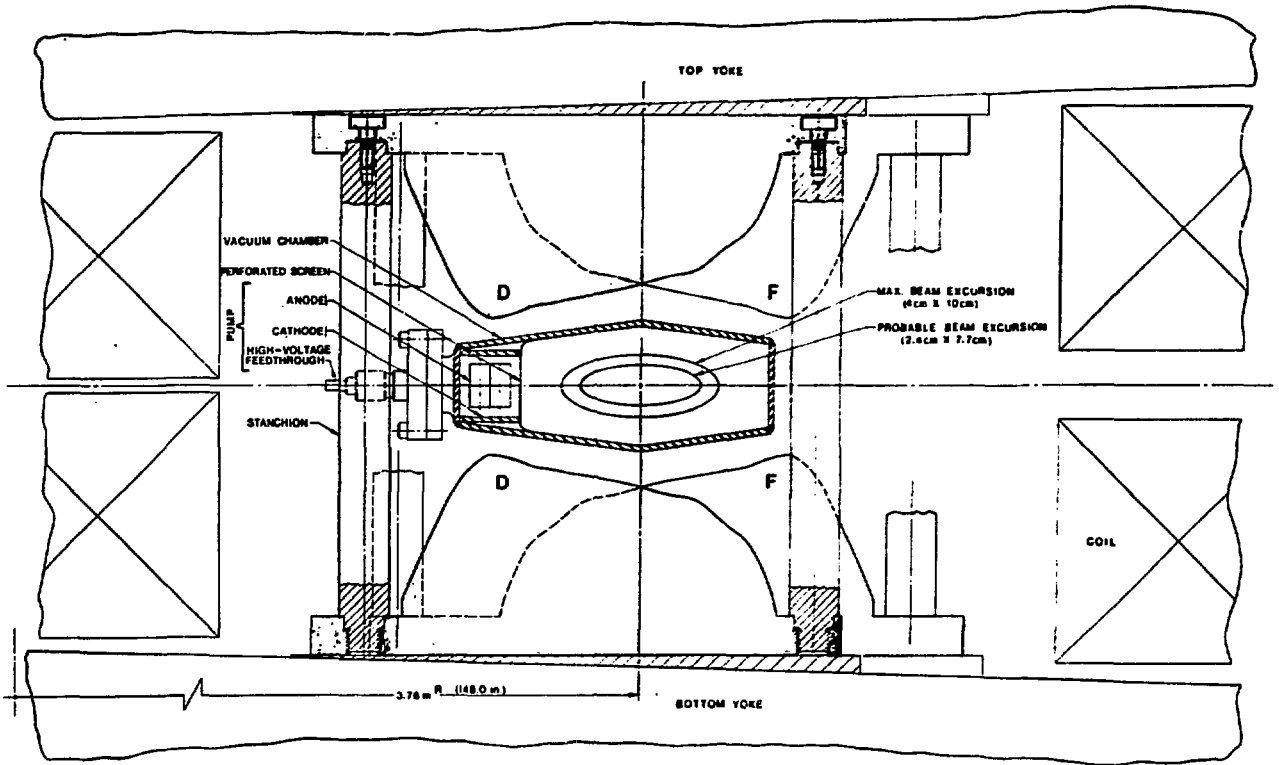

Fig. 3. Section through ring magnet.

future use of the PSR require stacking of the beam in longitudinal phase space, this aperture will be needed to accommodate the resulting energy spread. Such stacking may be useful at such time as injection periods exceeding 1 LAMPF macropulse are attempted as a means of reducing the beam current passing through the stripper medium.

As a result of the decision to kick the beam vertically and then extract radially, the vertical transfer matrix between the effective center of the kicker and the entrance to the iron septum should be chosen to provide a maximum vertical displacement, with the kicked beam being parallel to the median plane (for the subsequent deflection to be purely radial) at the entrance to the iron septum. These requirements are met for a vertical phase advance of $\pi/2$ with the iron septum starting at a vertical waist. The kicker should also be located at a point where the vertical amplitude function is large. These optimal conditions yield a transfer matrix between the center of the kicker and the iron septum of the form:

$$\begin{bmatrix} 0 & f \\ -1/f & 0 \end{bmatrix}$$

where $\beta_{kicker}\beta_{septum} = f^2$. It is exactly of the form of the vertical transfer matrix between the end point and the center of the π-2π insert. Thus, the kicker can be placed at the entrance to the insert with the iron septum starting at the midpoint, as shown in Fig. 2. However, the efficiency of this configuration is not large, as these points represent relatively low values for the vertical β function, but the efficiency will be adequate.

Once the decision has been made to place the PSR components as shown in Fig. 2, the central drift length should be 7 m to provide adequate clearance for reasonable septum fields. Two meters are required for the vertical deflection system (as will be discussed later). One-half of the 7 m is provided by the end drift of the 90° bending lattice. Therefore, the end drift length of the π-2π insert should be 1 m long. A number of inserts appropriate to the PSR lattice are given in Tables I and II of Ref. 20, and three configurations are sketched in Fig. 1 of that paper. The desired lengths in the central and end drift lengths may be met within a range of the radial magnification parameter m.

Thus, the radial beam size within the central drift space may still be chosen to achieve other objectives. One such objective would be to increase the spot size on the stripper foil for minimum power density. The spot size can be increased further by increasing the vertical amplitude functions at the stripper foil plane and also by increasing the radial and vertical emittances by injecting off the equilibrium orbit (or by injecting an unmatched beam). This method is used at the expense of beam brightness. For much experimental usage, it is desirable to maintain the emittances below 2π cm-mr in either plane. With this limitation, the only acceptable solution to reducing stripper foil power density will be to increase the betatron amplitudes at the foil.

Vertical amplitudes within the insert cannot be changed appreciably, and changes would not be desirable anyway because of the added cost for the extraction system. However, radial aperture in the long drift space is very much at our option through the choice of m. Assuming that the stripper is placed at the start of the central drift space, that is at $\bar{\beta}$, the power density on the foil is proportional to $(\bar{\beta})^{\frac{1}{2}}$ (or inversely proportional to m). Thus, the practical limit depends on the feasible limit of the quadrupole pole-tip fields. PSR aperture requirements are given in Sec. II.A.5.

2. Alternating-Gradient Pole Tips. One difficulty generic to the combined-function type of magnet system is the tendency toward interaction of the adjacent alternating-gradient pole tips, causing saturation of the edges. Since this saturation can lie near the median plane of the lattice, at the equilibrium orbit, it can cause an unpredictable distortion of the field and of the orbit. This problem is generally handled by chamfering the edges of the pole tips in this region. A wooden mockup of the PSR alternating-gradient cell is shown in Fig. 4, in which the large exposed side areas and the chamfered region can be seen. Chamfering, however, further complicates the pole-tip geometry calculations to a point where successive models and field-mapping iterations are necessary to achieve the desired fields.

An experiment for the PSR has been initiated, using the CIT magnet yokes, to aid in this pole-tip contouring and field mapping. Use of the CIT magnets

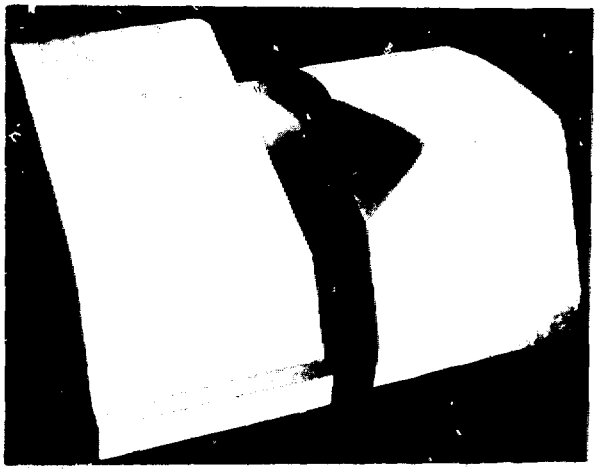

Fig. 4. Mockup of PSR alternating-gradient cell.

in a full-scale mockup will also be useful in uncovering engineering problems inherent in the ¼-scale Bevatron yokes, and will enable a full-scale test of the vacuum system which uses distributed ion pumps operating in the alternating-gradient fringing fields. The experiment will serve as a check on the feasibility of using the laminated synchrotron yokes in a direct-current application and indicate the resultant field quality.

This full-scale model will consist of enough yokes to set up a few cells for modeling, but not the entire 90° quadrant. It has been suggested that a temporary coil be made using pole-tip correction coil conductors to eliminate the need for large power supplies, high water-cooling requirements, and needless assembly of yokes to form the full quadrant. Cost of the material has been estimated at $5000 for the coils, and forming costs have been estimated at $4000.[21] Since the coil will be made from the same conductors as the pole-tip windings, and loosely formed without sharp bends, the $5000 material cost can be recovered. One standard LAMPF 600-A power supply can be used to power this most important machine development experiment.

3. Gradient Trim Coils and Lattice Tune Parameters. Another difficulty common to the combined-function type of magnet system is the tendency toward interaction of the gradient trim coils placed on the alternating-gradient pole tips with the main guide field. In fact, this interaction can shift the equilibrium orbit outside the PSR vacuum envelope. This effect can be reduced by careful dressing of the leads so as to average currents in the windings and to cancel their effect on the main field. Preliminary engineering has been completed on the pole-face correction coil design and a section showing the correction coil layout is given in Fig. 5. With a single layer of windings it is possible to achieve a ±5% shift in gradient with this method. By the addition of a second layer of windings a greater shift can be accomplished if desired. The wide-aperture CIT magnets give the designer considerable freedom in this regard and also allow ample room to dress the correction windings to minimize interactions. At present, the 5% swing will probably be sufficient for the PSR because the equilibrium orbit charge-exchange injection scheme is planned, rather than the complicated synchrotron or betatron stacking.

Available tunes for the PSR are given in Fig. 6. The operating point for PSR is shown to be $\nu_x = 4.36$ and $\nu_y = 2.34$. The operating region for the 5% shift in gradient is shown by the shaded region. The operation point has been chosen nearer (4.5, 2.5) rather than (4.0, 2.0) because the 2θ and 4θ harmonics are strongly driven due to the PSR periodicity, whereas the 5θ and 9θ can exist only as error fields.

4. Forbidden Tunes and the PSR Resonance Diagram. The equations of motion describing betatron oscillations include the main linear terms that provide the restoring forces, terms describing the magnetic field dependence on the particle's position, and may include additional terms. Under appropriate combinations of betatron amplitudes and frequencies, one or more of these terms can resonantly drive the betatron motion, frequently leading to loss of a portion of, or all of, the beam. The term in the Hamiltonian from which the betatron equations are derived (of the form $x^m z^n \cos k\theta$) will provide such a resonant term whenever $m\nu_x + n\nu_y = k$ (or $n \pm k$, $2N \pm k$, ...) where m, n, k are integers and N is the superperiodicity of the lattice.[22,23] The order of the resonance is $|m| + |n| - 1$. Simply stated, the lower the order the more dangerous the resonance and the faster the growth. For $|m| + |n| > 4$, resonances lead to loss only for particularly restrictive apertures because frequency-shifting terms move

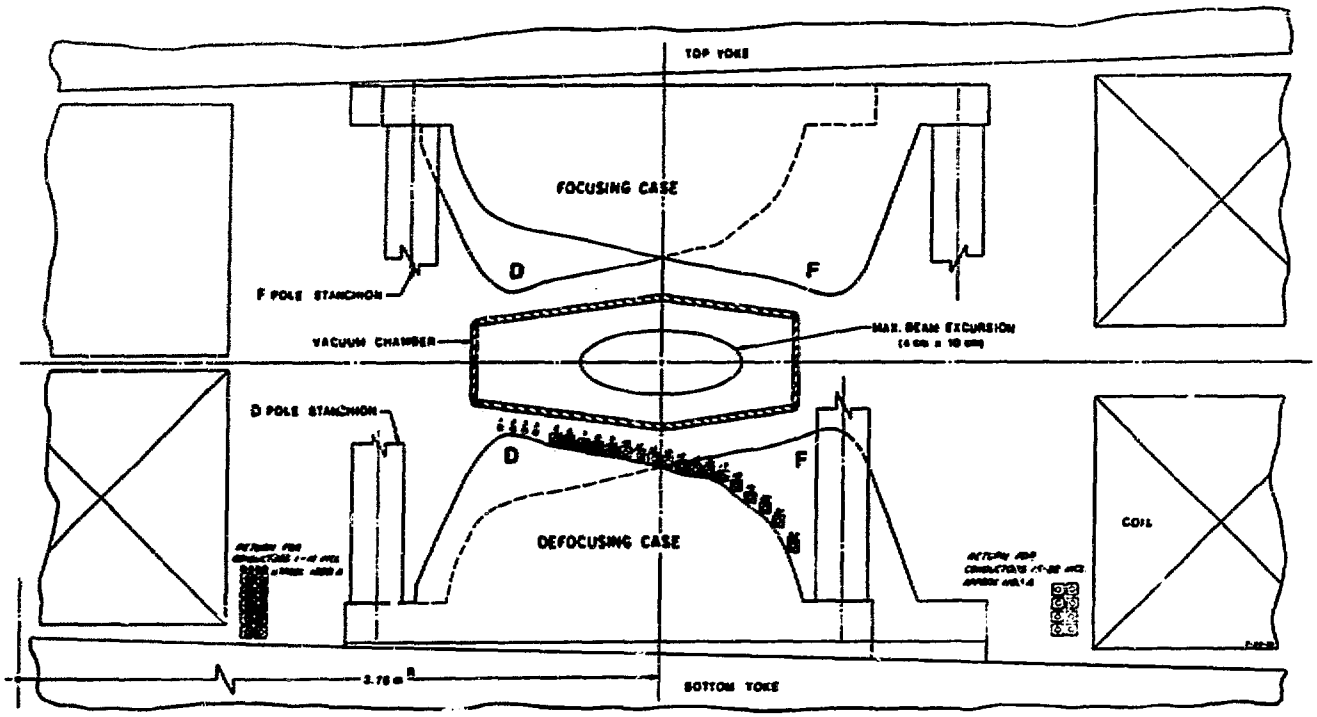

Fig. 5. Pole-face correction coil layout.

the particle out of resonance with increasing amplitude.

Those terms for which k is a multiple of N and which obey the design symmetry (i.e., n is even) are essential resonant terms, as they are obviously present; the corresponding resonances must be avoided. Other terms can occur only as the result of error fields and are thus expected to be of much smaller amplitude. However, the operating point cannot rest directly upon such a resonance because reasonable tolerances do not preclude the appearance of such a term.

The operating point must be chosen such that $|m\nu_x + n\nu_y - k| > \varepsilon_{mnk}$ for all integers m, n, and k. The safety margin ε_{mnk} (hopefully, small) increases with the amplitude of the driving harmonic and decreases with increasing order and increasing aperture. Figure 7 is a resonance diagram for the PSR. The operating point is chosen to be distant from the essential resonances, particularly those driven by the even harmonics of either the guide field or the magnetic field gradient. All close-by resonance lines represent error fields. Because of the low periodicity of the lattice, which is two, it is not possible to find a tune quadrant that does not contain essential resonances. Successful operation of SPEAR demonstrates that such is not necessarily optimum. Because PSR is a constant-field machine, it should be possible to reduce the magnitude of all error fields beyond the point where any resonant effects are observed. Due to short confinement times, weaker resonant phenomena are less important here than in the usual storage ring. The pole-face trim coils have adequate tune-variation capability to avoid any resonant difficulties that arise. For example, the $\nu_x - \nu_y = 2$ resonance is driven by the second harmonic of any residual skew quadrupole field.

By viewing such a resonance diagram, one soon realizes the tight constraints that are placed upon stable PSR operation. These constraints are further tightened and complicated, as will be seen later, by known beam-environment interactions and instabilities which place further limitations on the operating area, and certainly by unknown high-current interactions which will appear as the goals of the PSR are pressed. The discovery and means of overcoming these latter limitations will make development of the PSR a very exciting experimental program.

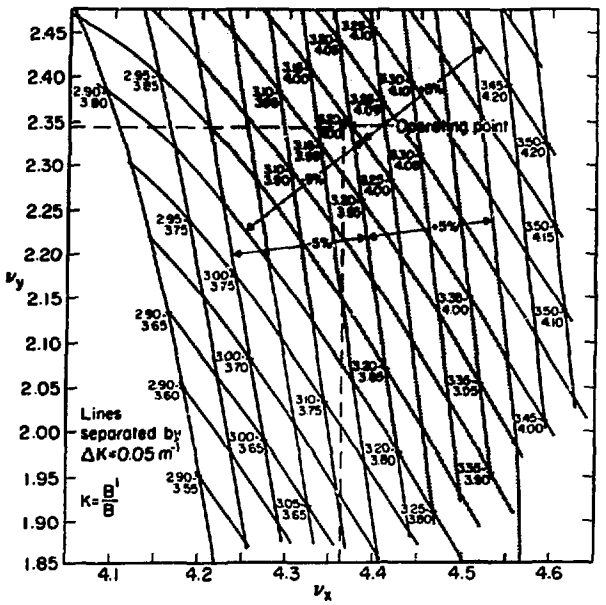

Fig. 6. Trim coil tuning chart (4-MHz period).

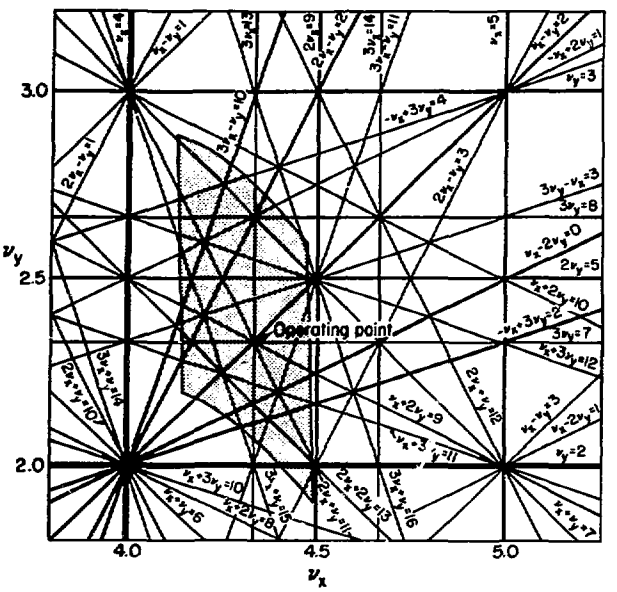

Fig. 7. WNRF resonance diagram and tuning chart. (Relative strength of resonance shown by line width. Operating region shown by shaded area.)

5. Closed-Orbit Deviations - Errors. Failure to align exactly each of the magnetic blocks in the PSR will result in a departure of the equilibrium orbit from the magnetic center lines. The alignment process to calculate the magnitude and statistical distribution of the departure of the magnet center lines from design positions is investigated, assuming reasonable tolerances for the required measurements. The amplitude response of the closed orbit beam to these misalignments can then be calculated. However, it is not the rms amplitude response but the maximum beam amplitude that determines the excess aperture requirements; therefore, we need to relate these amplitudes and their statistical distributions. The requirement is to ensure with a high probability (98.5%) that the maximum displacement of the equilibrium orbit resulting from misalignments will not exceed the available aperture allowance. These topics have been extensively studied by Laslett[24-27] and Smith[28,29]; and are well described in the LBL 200-GeV design study.[30] Because the PSR operates with a time-invariant magnet field, the accuracy in locating magnetic centers should greatly exceed that of conventional synchrotrons. Once a closed orbit is obtained, the measured deviations in this orbit can be used to improve the alignment of the magnetic structure itself.

For the PSR, components in the alignment process to be considered are: (a) monument placement accuracy, (b) transfer to magnetic centers, including errors in fiducial marks, and (c) field error in the magnets themselves. Stray fields are of no consequence in spite of the long straight sections because of the high guide field and the particle rigidity.

It should be possible to locate monuments accurately because of the relatively short distances and the basically simple geometry involved (that of a rectangle). However, a tolerance of 0.005 in. shall be used in applying the formulas IV.9b and 9c from the 200-GeV study. These formulas include the effects of monument-to-monument correlation and the correlation due to closure of the traverse around the monuments. For a 98.5% assurance of accommodating the resulting closed orbit, a 0.58-mm aperture in the radial plane and a 0.87-mm aperture in the vertical plane should be allowed.

Offset and fiducial errors provide the dominant contributions to closed-orbit displacement in the PSR. The appropriate formula from the 200-GeV study (IV:12) is:

$$\sigma_b = \frac{\pi \sqrt{\beta_{FF} <\beta>}}{\sqrt{2M}|\sin\pi\nu|} k\sigma_e \quad .$$

For the PSR, the maximum β in the gradient magnets are 5.5 m (x) and 9.7 m (y). The mean β are 2.3 m (x) and 4.3 (y). The average radius is 9.98 m, and the number of measurements is 28--that is, we position the ends of each of the 24 pole pieces with respect to the monuments.

In the 200-GeV study, the tolerances on offset measurement and fiducial mark locations were, respectively, 0.002 and 0.005 in; these statistically independent measurements are combined in quadrature to yield 0.14 mm. We should expect better tolerances on a direct-current magnet. Using these tolerances in formula IV.12 with a multiplier of 7 to yield the full-aperture allowance for 98.5% assurance of accommodating the resulting displacement yields:

$$2\,a_x = 7\sigma_{bx} = 40.7\,\sigma_e = 5.6 \text{ mm};$$
$$2\,a_y = 7\sigma_{by} = 75.7\,\sigma_e = 10.4 \text{ mm} \quad .$$

This last number ($2a_y$) is rather large; however, the aperture exists. Moreover, as reported in the LBL study, these coefficients may be large for particular lattice structures.

We could take advantage of the $M^{-\frac{1}{2}}$ factor and the CIT magnet lamination structure to increase the number of measurements to 21 per quadrant (using the lamination breaks). With M = 84, the aperture requirement is reduced nearly 50% (about 5 mm in the vertical plane).

For the calculation of the effect of field errors, one again uses the approach in the LBL 200-GeV study. We find that for an error in B_y of one part in 10^4, there is a 98.5% assurance that the resulting radial excursions of the closed orbit will lie within a full aperture allowance of 1.6 mm. For similar field errors in the median plane, i.e., $<B_x> = 10^{-4}B_o$, which is probably large, the 98.5% assurance of accommodating dips and rises in the median plane will require a full (vertical) aperture allowance of 3.0 mm. A summary of aperture requirements is given in Table III.

TABLE III

SUMMARY OF APERTURE ALLOWANCES[a]
FOR 98.5% ASSURANCE OF ACCOMMODATING FLUCTUATIONS

Cause	Tolerance	a_x (mm)	a_y (mm)
Error fields $\Delta B_y/B_o$ ($\Delta B_x/B_o$)	1 in 10^4	1.6	3.0
Monument location errors	0.005 in.	0.58	0.87
Fiducial and transfer errors	0.002 in. 0.005 in.	5.6	10.4[b]
Stray fields	-	nil	nil

[a] Each of these full-aperture allowances is statistically independent of the others; therefore, we combine them in quadrature to obtain the overall allowance required for 98.5% assurance of accommodating the closed orbit perturbations;

$2\,a_x = 5.8$ mm; $2\,a_y = 10.9$ mm (or 6.1 mm if 4.5° interval is used in the leveling of the pole pieces)

[b] 5.2 mm if measured every 4.5°.

Experimental requirements limit both radial and vertical beam emittance to 2π cm-mr. Thus, the maximum betatron amplitude within the magnet structure is 1.05 cm for x and 1.4 cm for y. The maximum synchrotron amplitude for $\Delta p/p = \pm 0.2\%$ is 0.22 cm. Adding the error aperture allowances yields 3.1 cm for the required radial aperture and 3.9 cm (or 3.4 cm for 4.5° interval) for the vertical aperture.

In the case of random field error it will be necessary for $\Delta B_o/B_o$, the relative field error, to not exceed 0.01% (ΔB_y for x, and ΔB_x for y) to keep the equilibrium orbit within 2 mm radially and 3 mm vertically. Any 2θ component of the median plane twist (B_x field) will mix radial and vertical planes as a result of the $\nu_x - \nu_y = 2$ resonance. However, no instability will occur. In order not to drive the the resonance $3\nu_x = 13$ and $\nu_x + 2\nu_y = 9$, the 9θ and 13θ components of the sextupole field should be avoided (these are error fields). The 5θ and 9θ errors in the gradients should also be avoided (these are error fields and they will open the stop bands $2\nu_y = 5$ and $2\nu_x = 9$, respectively, on the resonance diagram).

6. PSR Chromaticity and Sextupole Correction Requirements. Without correction, the designed radial and vertical betatron frequencies will apply

only to protons of exactly 800 MeV. Particles of slightly different energies, as a result of their different rigidities and equilibrium orbits, experience different amounts of focusing. The shift in tune resulting from a shift in energy can be easily calculated from second-order terms in a power series expansion of the radial and vertical displacement and slopes at some turn n in terms of the displacements, slopes, and momentum shift at turn n-1. From these expansions, we can also determine the momentum shift that carries the beam into instability and the increase in the betatron amplitude that accompanies a momentum shift. Finally, one can determine the sextupole field distribution that is needed to eliminate these effects.

Starting with power series expansions about the design-momentum equilibrium orbit, we expand about the equilibrium orbit for momentum (p + Δp) to obtain the single-turn transfer matrices about this closed orbit. In the absence of sextupole correcting fields the tune shift for the PSR is

$$\partial\nu_x/\partial(\Delta p/p) = -2.95;\ \partial\nu_y/\partial(\Delta p/p) = -5.89 \quad .$$

The stability range, based on the radial plane for the PSR, is

$$-2.47\% < \Delta p/p < 11.83\%;$$

whereas for the vertical plane it is

$$-1.14\% < \Delta p/p < 6.40\%.$$

At the F-F symmetry point, β_x is doubled for $\Delta p/p$ = 15%, whereas β_y is doubled for $\Delta p/p$ = 1.3%.

A sextupole field of 5.188 B_o/m^2 in the focusing magnets and -10.147 B_o/m^2 in the defocusing magnets of the curved portion of the lattice eliminates the tune shift (Table IV), except for the higher order terms. Moreover, this correction reduces the change in the β functions by an order of magnitude.

TABLE IV

CHROMATICITY AND SEXTUPOLE CORRECTIONS

	After Correction	Before Correction
Radial Plane:		
$\frac{\partial m_{11}}{\partial(\%\Delta p/p)} = 2 \cdot X_{eq} \cdot T_{111} + T_{116}$	0.000016	0.08381
$\frac{\partial m_{12}}{\partial(\%\Delta p/p)} = X_{eq} \cdot T_{121} + T_{126}$	0.01389	0.01032
$\frac{\partial m_{21}}{\partial(\%\Delta p/p)} = 2 \cdot X_{eq} \cdot T_{211} + T_{216}$	0.02178	0.1697
$\frac{\partial m_{22}}{\partial(\%\Delta p/p)} = X_{eq} \cdot T_{221} + T_{226}$	0.000025	0.08381
Vertical Plane:		
$\frac{\partial m_{11}}{\partial(\%\Delta p/p)} = X_{eq} \cdot T_{313} + T_{336}$	-0.000034	-0.1695
$\frac{\partial m_{12}}{\partial(\%\Delta p/p)} = X_{eq} \cdot T_{314} + T_{346}$	-0.007427	-0.00385
$\frac{\partial m_{21}}{\partial(\%\Delta p/p)} = X_{eq} \cdot T_{413} + T_{436}$	0.05719	0.6680
$\frac{\partial m_{22}}{\partial(\%\Delta p/p)} = X_{eq} \cdot T_{414} + T_{446}$	-0.000020	0.1694

B. PSR Injection System

1. Negative Ion Source. The decision to use negative hydrogen ion injection for both modes of PSR operation circumvents many storage ring difficulties and complexities, such as synchrotron and betatron stacking.[31] Generally, such a decision results in the trade-off of known complexities in one field for unknowns in another. In this case, however, this is not true. Ample precedent exists for this type of operation, and the technology of negative-ion-source development has advanced to the point where the full potential of LAMPF to accelerate 17 mA of H^- can be realized. Charge-exchange injection for storage rings has been described by Dimov, and ANL has demonstrated the important bonus of attaining 100 times the stored beam brightness which could be achieved using conventional injection methods--a highly important feature to WNRF.[32]

Considerable evidence exists that a negative hydrogen ion source, capable of producing 17-mA intensity within the LAMPF admittance requirements, can be developed.[33-35] Such a development program has been initiated at LASL. In a recent LASL collaboration with Brookhaven National Laboratory (BNL), cesium was injected into the interior of a hollow arc duoplasmatron ion source (described in Ref. 36). The directly extracted H^- current increased by a factor of 2-2.5. Since that time, the BNL group has reportedly observed 13-15 mA of H^- (pulsed) from this type of source. This is an enhancement factor of 2-3 over H^- currents typically extracted from this ion source prior to the introduction of cesium.[37,38] Thus, the negative ion source development program appears to be already approaching the 17-mA goal.

As may be seen from Table I, use of the full 17-mA H^- current would be rewarding in several ways. First, it would allow new options for pulse-mode operation. The 17-mA H^- beam (unbunched) would be accelerated to 750 keV and then chopped into a pulse train in the H^- low-energy transport system using a distributed transmission-line deflection system similar to that being developed for WNRF proton operation. This pulse train would consist of 5-nsec-wide pulses spaced every 50 nsec. Every tenth rf bucket of LAMPF would be loaded and the resultant beam injected into the PSR. This pulse train would synchronously overlay and add to the five bunches circulating in the PSR in this mode. The single PSR 201.25-MHz rf cavity operating at a peak voltage of 100 kV will retain this structure.

An alternative to chopping a 17-mA H^- beam for pulse-mode operation would be to bunch inside a modified 1.7-mA negative ion source by a factor of 10. A 3-keV H^+ beam could be generated by an ion source (of the Lawrence Livermore Laboratory (LLL) type) having a multiple-aperture extraction system. This beam would then be transformed into an H° (neutral) beam in a cesium vapor charge-exchange cell. The cross section for H° formation is extremely large at this energy ($\approx 10^{-14}$ cm^2/atom), so that nearly all the emergent beam would be H° atoms. This beam would then be allowed to drift approximately 1 m to a second charge-exchange cell containing sodium vapor where 10% would be converted to H^-.[39] Suitable trapping procedures would prevent contamination of LAMPF by alkali vapor. Modulation of the H^+ extraction system with a 20-MHz ramp waveform having an amplitude of 200 V would accomplish bunching. This has the effect of modulating the velocity of the drifting H° ions by a sufficient amount to produce 20-MHz bunching of the beam at the end of the second charge-exchange cell. If the energy spread in the initial beam due to the finite ion temperature in the H^+ source is less than 20 eV (it should be considerably smaller than this in practice), then each 50-nsec interval of beam will be compressed into a beam of less than 5 nsec at this point. Thus, such a modified 1.7-mA H^- source could be used to produce a train of pulses 5 nsec wide every 50 nsec to load every tenth bucket of LAMPF. Since the 1.7-mA H^- beam would be compressed a factor of 10 in the ion source, it would be equivalent to a chopped 17-mA H^- beam.

Development of the full LAMPF potential to accelerate 17 mA of negative hydrogen ions would have additional important advantages, especially for high-current operation of the PSR. Should this level of H^- current be used, rather than the LAMPF design goal of 1.7 mA, the loading time for 34 A of circulating current in the PSR would be reduced by a factor of 1/150 (1 macropulse rather than 3). Since growth time for instabilities would be reduced by the same factor, this will be highly important to the realization of PSR high-current goals, as we shall see in the section on (known) instabilities. In this mode of operation the PSR will be operated slightly asynchronous with respect to LAMPF to prevent pile-up of micropulses and to ensure a direct-current distributed beam. This kind of operation will circumvent possible unknown instabilities due to high-current pulses. This is basically the reason for the decision to load the PSR in a direct-current manner for the high-current mode, thus relying on the precedent of high direct-current containment--rather than operating in the unexplored field of high-current pulse containment.

2. Negative Hydrogen Stripper System. The PSR operation with charge-exchange injection contains several practical injection schemes, although all schemes suffer from final stripper power density limitations for high PSR current operation. One possible system would be to use a magnet in the PSR lattice which would cause the entering H^- ions to follow a mirror image path of the protons circulating in the ring and then be stripped to form protons at the point where the H^- and H^+ beams become tangent. The danger of this type of injection is that, unless the magnetic fields are kept small, a superperiod of one can be induced in the ring, leading to instabilities. With a low field convergence magnet the injection angle must be small, and this can interfere with the large CIT yokes. Nevertheless, this system is a practical solution and is in use at ANL.

a. H^-→H° Injection Across PSR Field. The alternative to mirror-image injection is neutral beam injection. The negative ions are first stripped to neutral atoms and then drifted through the CIT lattice onto the PSR equilibrium orbit, where they are stripped to protons and stored. The problem here

is to find a practical method of accomplishing the $H^- \rightarrow H^\circ$ transition which causes a minimum of (undesirable) increase in the beam emittance. The thrust of LAMPF Machine Experiment 128 is to investigate possible material stripper atomic cross sections and methods for accomplishing these transitions. Chief among the methods to accomplish the first transition are the use of a magnetic field step to effect the $H^- \rightarrow H^\circ$ transition, and the use of flash lamps to remove the electron via photo detachment. The first method will substantially increase the emittance of the beam.[40,41] The second method would not suffer from this problem but probably the repetition rate will be limited.[42] The proper course to follow must await the results of the above-mentioned machine experiment.

b. $H^\circ \rightarrow H^+$ Transition Inside PSR. The concept of H^- charge-exchange loading of the PSR requires a rather careful examination of foil temperatures, for the final foil must intercept all of the PSR circulating beam (unless orbit perturbation methods are employed). The problem is to determine a rather accurate prediction of foil temperature from which one can choose an appropriate configuration, estimate foil lifetimes, and peak PSR stored currents. Carbon appears to be the best suited for initial PSR operation, because of its large specific heat, high emissivity, high melting point, low-Z, and its availability in thin foils. The subsequent discussion will be limited to this material used as a stripping foil--either stationary or mounted on a rotating disk in a fashion similar to the ANL system.[43]

Energy is deposited in the foil from two sources. The first and smaller of the two is the energy loss of the stripped electron (Q_e), occurring only during the injection cycle of the beam and not during subsequent passes of the stored proton beam through the foil. Assuming $\beta_e = \beta_{H^\circ}$, the initial kinematic energy of the stripped electron is 436 keV (E_{H° = 800 MeV). Figure 8 shows the energy loss of the stripped electron as a function of foil thickness. A simplifying assumption that will overestimate Q_e but not appreciably affect the foil temperature calculation is that the electrons are stripped on the entrance face of the foil and subsequently pass through the entire stripper. Q_e is then given by

$$Q_e = \frac{V_e(x) I_o \Delta t_i}{J} \quad \text{cal} \quad ,$$

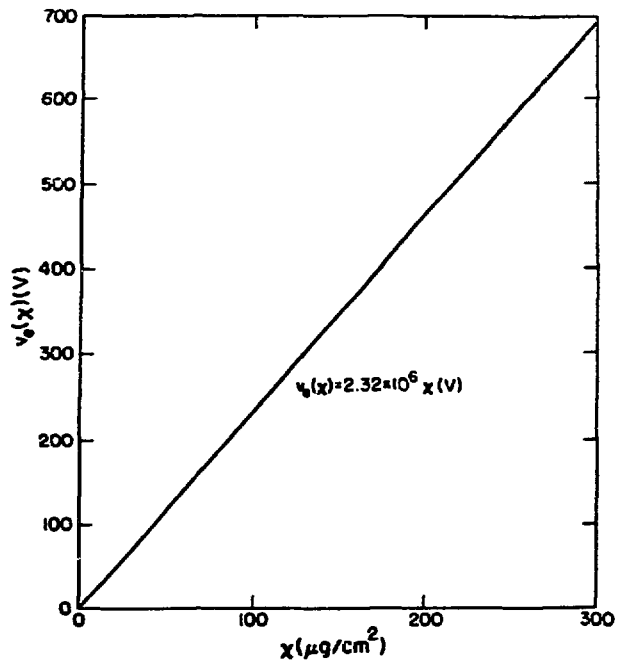

Fig. 8. Energy loss of 436-keV electrons in carbon.

where $V_e(x)$ is the energy loss of the electron in a foil of thickness x, I_o is the injected current, Δt_i is the injection time, and J is the mechanical equivalent of heat.

The second source of energy deposition in the foil is that deposited by protons (Q_p). At first glance, it appears that this should be just the loss of energy of the proton beam. However, recent calculations of δ-ray losses from thin foils indicate that a modest fraction of proton energy is carried out of the foil by these rays.[44] Unfortunately, these calculations are nonrelativistic and extend only to 50 MeV.

As a result, new calculations have been made using a semirelativistic δ-ray production cross section. Figure 9 shows the fraction $\psi_\delta(x)$ of proton energy loss removed from the foil via delta rays. The incremental heat lost by the protons is then

$$\Delta Q_p = \frac{n I_o \Delta t_o}{J} \frac{dE}{dx} \times \{1-\psi_\delta(x)\} \quad \text{cal} \quad ,$$

where n is the number of turns injected into the ring, I_o is the injection current, Δt_o is the ring period, and dE/dx is the usual proton energy loss.

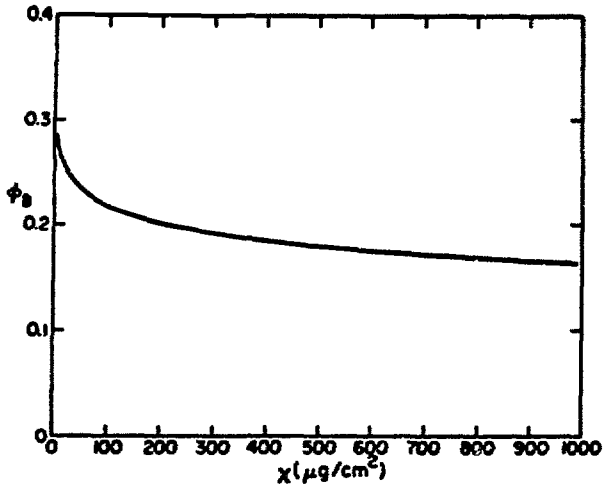

Fig. 9. Fraction of energy removed by δ rays vs foil thickness (carbon foil, E_p = 800 MeV).

It is next possible to write the energy balance equation for the foil

$$\Delta Q_e + \Delta Q_p = xA\,C(T)\Delta T + 2\sigma\varepsilon A(T^4 - T_o^4)\Delta t + \Delta Q_{T_e}(T) \quad .$$

Terms on the left of this equation are energy source terms, while those on the right are sink terms. The first term on the right is the specific heat, xA is the foil mass being heated (m = xA, A the beam area), C(T) is the specific heat of the foil. Its dependence on temperature T is displayed in Fig. 10. The second term is the radiative cooling term; σ is the Stephan-Boltzmann constant, ε is the emmissivity, and T_o is the temperature of the foil surroundings. The factor of two arises from the fact that cooling is effective from both faces of the foil. The final term represents energy carried away by thermionic electrons. Thermionic cooling is not an important effect below 2700°C. In addition, 50-100 thermionic electrons must be emitted to carry away the energy deposited by a single proton. Because tens of amperes of current are required to achieve such high temperatures, the thermionic current is kiloamperes and the resultant ohmic heating is two orders of magnitude greater than ion heating. Thus, thermionic cooling systems seem impractical, and the last term in the above equation can be set to zero. It should be noted that in many instances inclusion of the specific heat term is vital to the calculations, for it not only reduces the peak temperatures but also also elevates the minimum temperatures.

Because of its complexity, the above equation does not lend itself to an analytical solution, and must be evaluated by numerical (computer) techniques. Calculations to date assume a uniform beam current density over the area and ignore thermal conduction in the plane of the foil. To evaluate this equation, a suitable foil thickness must be assumed. Accurate determination of this thickness will evolve from LAMPF Machine Experiment 128. For the present calculations, the estimate of 262 $\mu g/cm^2$ for 99% stripping will be used.[45]

The best location in the PSR for the stripper foil is where the beam divergence is largest, so as to minimize the emittance growth of the beam due to repeated passes through the foil. However, beam area should be as large as possible to minimize power density on the foil. Unfortunately, these requirements are mutually exclusive. A location meeting the above boundary conditions to some extent is at the exit from the third quadrupole on the injection straight section of the PSR. A beam area of 2.9 cm^2 will be assumed at this point, and should be readily attainable with the LAMPF emittance and the variable π-2π insert magnification (1-10) available there.

Figure 11 shows foil temperature as a function of time in the pulse-mode of operation. Beam is injected at 1.7 mA for 50 μsec (stored pulse peak current 3.4 A) once during each LAMPF macropulse. After five cycles, the foil temperature has stabilized, cycling between 1050 and 925°C. On the basis

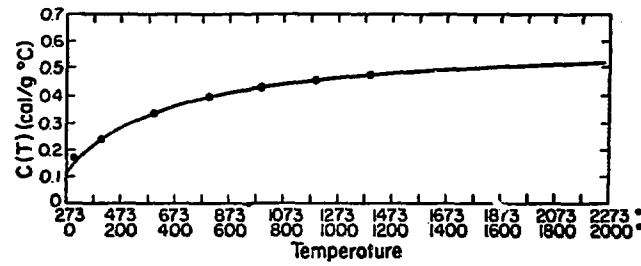

Fig. 10. Specific heat of carbon (graphite). (Circled points taken from Nuclear Engineering Handbook.) $C(T) = 0.590 - \frac{178.6}{116.3 + T(°K)}$.

of thermal considerations, the foil should last almost indefinitely at these temperatures.

Figure 12 shows foil temperature as a function of time for the high-current mode. In this mode, peak foil temperature would be high if a single foil of thickness 262 $\mu g/cm^2$ were used. Six foils of 30 $\mu g/cm^2$ thickness mounted at 45° with respect to the beam and placed 10 cm apart would increase the radiating surface by 8.5, reducing the equilibrium temperature by approximately 1.7. Curve A of Fig. 12 traces the foil temperature while 10 macropulses of

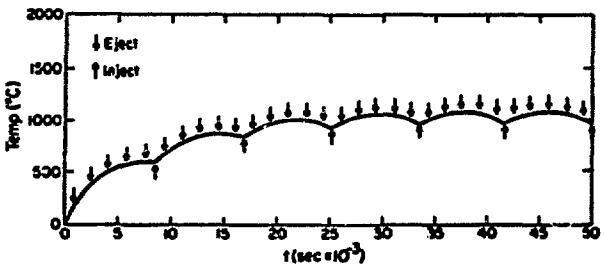

Fig. 11. Carbon foil temperature low current, high-duty mode. 262 $\mu g/cm^2$, I_i = 1.7 mA for 50 μsec. Stationary foil, beam undeflected, 3.4 A stored (peak).

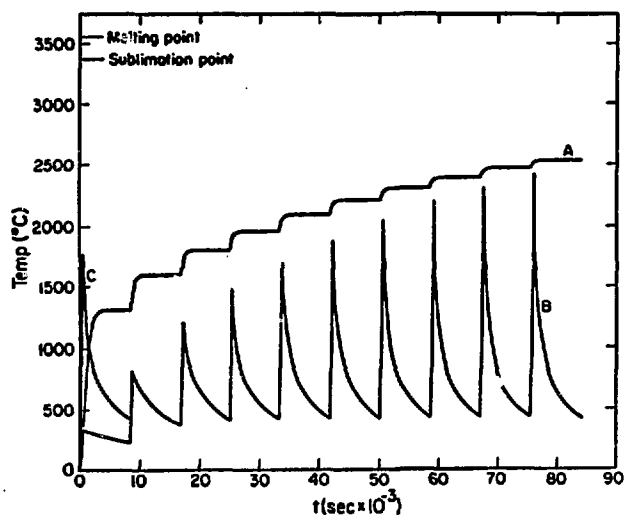

Fig. 12. Carbon foil temperature to store 34 A. Curve A: I_i = 1.7 mA 30 $\mu g/cm^2$ at 45° stationary foil, undeflected beam. Curve B: I_i = 1.7 mA 30 $\mu g/cm^2$ at 45° stationary foil, deflected beam. Curve C: I_i = 17 mA 30 $\mu g/cm^2$ at 45° stationary foil, deflected beam.

average current 1.7 mA are being loaded into the PSR to attain a stored current of 34 A. At the end of the injection, the foil temperature reaches 2520°C and, shortly thereafter, the equilibrium temperature of 2536°C. This is well below the carbon sublimation temperature of 3367°C. Even at 2536°C, for the full injection time of 75.5 msec, the foil thickness would only be reduced by 2% from evaporation.

Curve B traces the foil temperature under the same conditions, except that the beam is deflected from the foil between macropulses (either by a shift in the equilibrium orbit or the use of a spinning foil wheel similar to that used by ANL). This method allows the foil to cool between successive macropulses. In this case, the equilibrium temperature is only slightly lower (2414°C) and the thermomechanical stressing is more severe than for stationary foils. The primary advantage of this technique is that the number of passes of the proton beam through the foil is 0.06 of that for Curve A and hence the rms angular spread of the beam due to the foil is reduced by a factor of 0.245.

Curve C shows the foil temperature history when the PSR is loaded with 17 mA of H^-. In this case, the 34-A circulating current can be attained in 1 macropulse and therefore the temperature is only 1761°C. In this case, the rms angular divergence introduced by the foil is reduced from that of Curve B by a factor of 0.316 and from that of Curve A by a factor of 0.077. This underscores further the need for a 17-mA LAMPF H^- beam capability.

In Fig. 13, the foil temperature is traced to ultimate thermal destruction. Curve A (a continuation of Curve C, Fig. 12) slightly exceeds the sublimation point at the end of injection of the third macropulse. If the foil survives this, it will reach the melting point for carbon partway through the injection of the fourth macropulse, when the stored current reaches 122 A. Curve B traces the time history of the hottest portion of a rotating foil (the trailing edge). Rotation not only removes the foil from beam exposure between macropulses, but also increases the irradiated surface by streaking it. At a foil speed of 400 m/sec (such rim velocities can be obtained with good disk design practice) the foil strip would be about 20 cm long. Pyrolytic carbon foils can now be obtained

in thicknesses of approximately ¼ mg/cm^2. Pyrolytic carbon possesses a high tensile strength (40,000 psi) and retains this strength to temperatures in excess of 2760°C.[45] For the above velocities, this corresponds to a safety factor of approximately 18 X. Curve B exceeds this temperature during the injection of 5 macropulses with 170-A stored current.

At the highest temperatures, the above calculations could be in error by as much as ±50%; nevertheless, the pulse-mode specification of 3.4-A peak and the high-current mode specification of 34 A should be readily attainable with simple carbon stripper foil configurations.[46] The high-current goal of 100 A should be attainable with more sophisticated foil strippers. Ultrahigh currents can be attained by foils and orbit stacking or by use of gas strippers.

The purpose of this report is to present a description of a basic PSR system capable of meeting immediate WNRF goals, and not to describe alternatives in detail. Alternatives and variations will evolve from the implementation of the various storage ring development experiments and the PSR mockup. However, two alternative final strippers are worth noting. A stationary gas cell (probably filled with H_2) can be inserted in the straight section of the PSR, thereby eliminating the problem of foil temperature for high-current operation. Such a cell faces a compatibility problem with the high vacuum requirements of PSR operation. Another difficulty would be the vacuum bump caused by the linear extent of such a cell. Foils also cause a density bump or discontinuity, but at least such a discontinuity can be confined to the region of a narrow beam waist, thereby minimizing the increase in beam emittance.

Another alternative, that of a gas jet target (again, probably H_2), warrants mention here.[47] This system, employed as the final stripping medium in the PSR, would be of more limited spatial extent. However, the same vacuum incompatibility, requiring heroic pumping and trapping measures, would result. On the other hand, it may be that the only feasible method of attaining the ultimate high-current goals of PSR operation will be to use a gas stripper medium at the expense of these trade-offs.

C. PSR Extraction System

The PSR extraction system must be capable of performing in the two operational modes of the machine. The more difficult of these is the pulse mode, in which it is desired to extract individually each of the five circulating bunches of protons with sufficient time elapsing between pulses for the WNRF time-of-flight apparatus to be able to record the slowest neutrons generated. The 50-nsec interval between the pulses circulating in the PSR is not sufficient, except for special types of spectrometers, and would lead to pile-up of information.[48] Therefore, the kicker must turn on in less than 40 nsec, remain stably at maximum voltage for at least 10 nsec, and turn off in less than 40 nsec without ringing (so as not to disturb the other bunches which are still circulating). The duty cycle requires that the kicker be able to perform repeatedly at 600 times/sec. Thus, less than 2 msec are available for power supply recovery. It is these pulse-mode engineering requirements that have pressed power supply and kicker design, but indications are that pulse-mode problems are now within the state of the art.[49] A kicker development program will no doubt have to be instituted, preferably in advance of PSR construction.

Kicker operation in the high-current mode of PSR operation is less demanding. The kicker must be able to turn on as fast as possible to minimize radiation spill during beam ejection. It must stay on to accomplish single-turn extraction of the direct-current beam circulating in the PSR (about 250 nsec). There are no requirements on turn-off characteristics

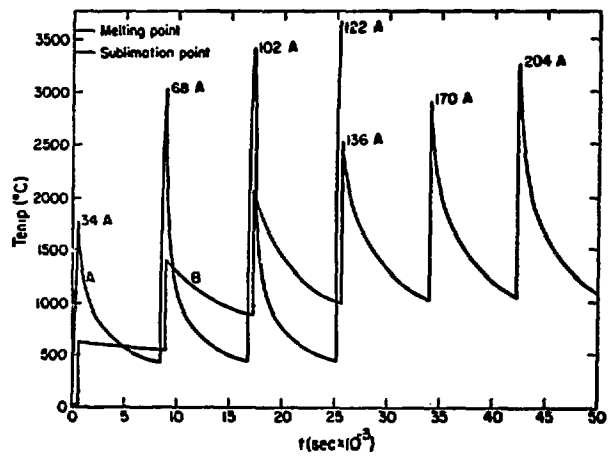

Fig. 13. Carbon foil temperature for maximum stored current. Curve A: I_i = 17 mA, 30 μg/cm^2 at 45° stationary foil, deflected beam. Curve B: I_i = 17 mA, 262 μg/cm^2 at 0° rotating foil (400 m/sec).

because there is no beam left to disturb. The kicker may use the entire 8 msec of LAMPF to recover.

For a detailed discussion of kicker extraction geometry and septum design for PSR, the reader is referred to the extensive study by Avery, LBL.[50,51] The basic geometry shown in Figs. 14 and 15 consists of a vertical kick of about 12.5 mr at the start of the long straight section insert. This is a focal point for the beam. Upon emerging from the third quadrupole in the insert, the beam is displaced 3.4 cm from, and is approximately parallel to, the undeflected beam. The extracted beam enters an iron septum in the long, central drift space. This septum then deflects the beam radially by 156 mr (9°) in a distance of 290 cm. At the exit of the septum the beam is displaced radially 30.4 cm, and enters a conventional transport system which leads to the WNRF transport line and ultimately to the WNRF neutron-producing target. Because the extracted beam consists of protons, 15-kG magnets can be used which are similar in design to those of WNRF.

The vertical kicker consists of two parallel conductors, above and below the median plane, 108 cm long and separated by 2.76 cm. The vertical kick is accomplished with a horizontal field of 610 G. The iron septum provides a vertical field of 2.62 kG. Flux is divided evenly at the center, which need be only 8 mm thick. Septum thickness increases with radial displacement to accommodate the accumulated return flux. With this geometry a large aperture is available for the deflected beam, but the leakage field is no greater than 3.2 G.

D. PSR Vacuum System

1. General Description. The ability to operate at UHVs of the order of 10^{-10} torr has proved most useful in attaining the CERN ISR stored-current goals. From its inception, CERN has found the luminosity of its ISR beam primarily limited by vacuum deterioration from chamber bombardment by the ions formed in high-current residual gas collisions.[52] Early in the WNRF/PSR study it was obvious that we needed an engineering study to combine the best features of a distributed ion pumped extruded aluminum chamber such as that in use at SPEAR, with the virtues of a bakeable stainless-steel system. The capability of shifting to UHV operation in an

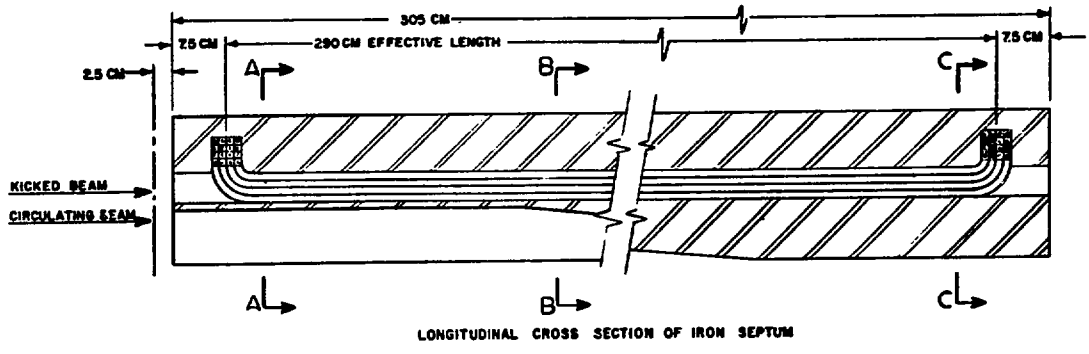

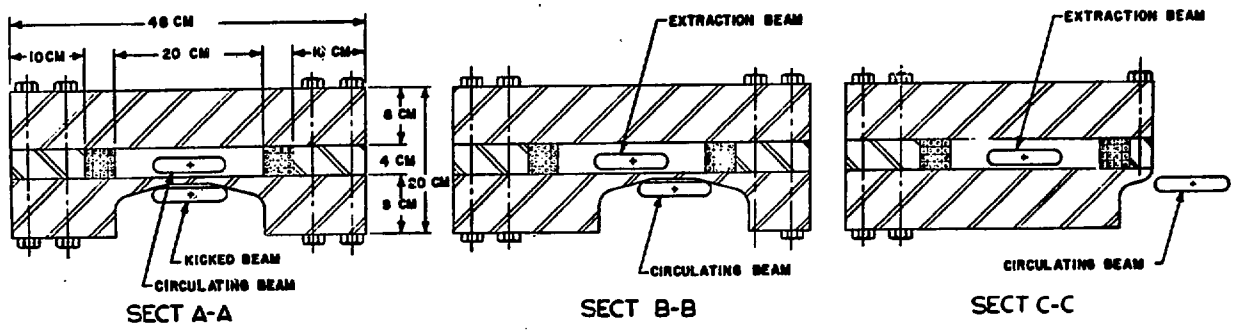

Fig. 14. Top: Longitudinal cross section of iron septum.
Bottom: Transverse cross sections of iron septum.

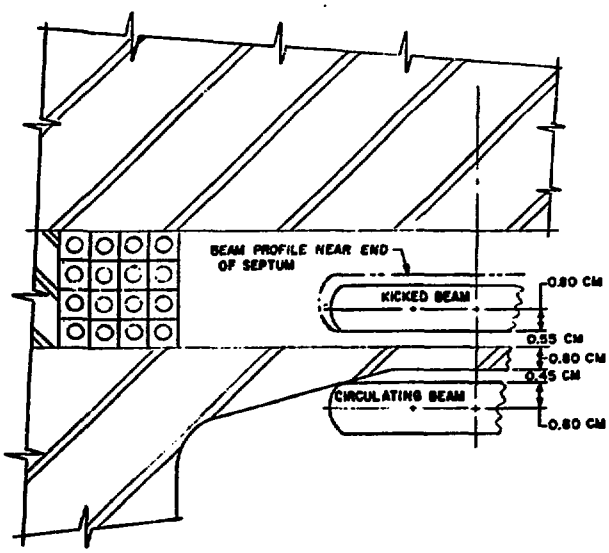

Fig. 15. Detail cross section near entrance of septum.

Fig. 16. Stainless-steel vacuum chamber showing welding jigs.

experimental machine such as the PSR (if it becomes necessary in the pursuit of high-current containment) would be essential, provided that the geometry of the curved chamber would not contain so many welds that fabrication costs would be prohibitive. Such a study has culminated in the beautifully simple, all-stainless-steel chamber shown in Figs. 16 and 17. Note that the curved chamber is fabricated without radial welds. Continuous distributed-ion pumps following the SPEAR design are shown in Figs. 18 and 19. These pumps have been adapted to the all-stainless-steel chamber and are held in place on the inner curve of the chamber by tension. Distributed-ion pumps allow continuous uniform pumping around the curved sections, thereby reducing the likelihood of vacuum bumps which have been shown to cause beam instabilities at the CERN ISR. Ultimate vacuum capability of this system when operating in an alternating-gradient field will be demonstrated in the full-scale mockup of a few PSR cells by insertion of the fabricated chamber and blanking it off. The system has been designed for initial operation at a highly reliable (oil-free) vacuum of less than 10^{-9} torr average pressure, without the use of rotary pumps. The vacuum envelope consists of four straight sections of round 16-cm-diam tubing having a total length of approximately 35 m, plus four curved sections or quadrant tanks having a center-line length of approximately 25 m, the cross section of which may be described as a nonregular hexagon. The vacuum envelope has a volume of approximately 935 liters and an outgassing surface area of about 29 m^2 (including pump manifolds).*

The UHV system will be all metal** (including seals) and will be provided with electrical resistance heaters and thermal insulation to permit in situ bakeout to 350°C. Convoluted bellows will be welded to each end of the straight sections, and transition pieces will be provided between round and hexagonal cross-section elements to eliminate discontinuities believed to upset image currents in chamber walls. Type 316 stainless steel has been chosen for fabrication of the curved tanks because it retains nonmagnetic properties after cold work, welding, and vacuum heat treat cycles,*** and is free of cracking--sometimes a problem with other alloys.

A gate valve in each straight section facilitates leak-hunting and permits quicker return to deep UHV should vacuum be intentionally broken.

*Does not include rf cavity, vertical kicker, injection or extraction system.

**Chemically etched and polished surfaces, viz., DiVersey DS-9, or equal.

***Prototype vacuum envelope sector 16K3326 degassed 5 h at 750°C during fabrication.

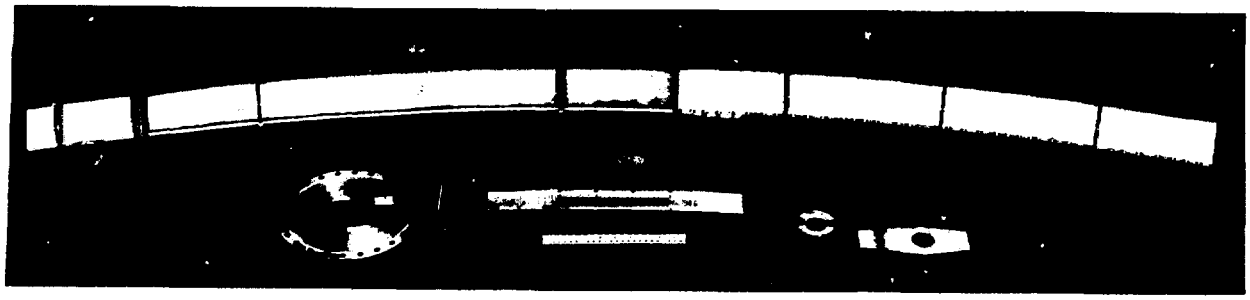

Fig. 17. Stainless-steel vacuum chamber.

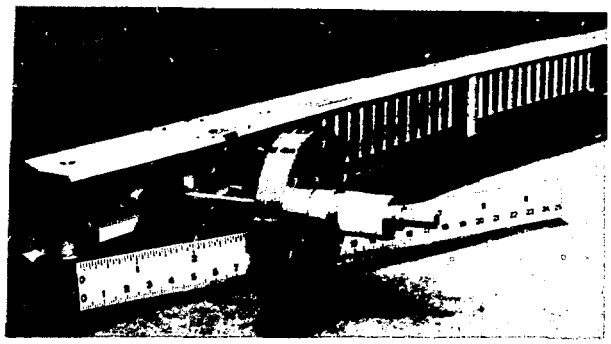

Fig. 18. Distributed-ion pump.

Pumping is accomplished in four stages with a combination of commercial and custom pumps. External pumps are grouped into six identical manifolds (Fig. 20). Each manifold consists of one vertically disposed commercial triode-type noble sputter-ion pump (air rated at 400 liters-sec^{-1}) plus three standard double-size liquid-nitrogen-cooled sorption pumps. Previously considered turbomolecular pumps are contraindicated at pressures below 5 x 10^{-9} torr.

Each ion pump is to be equipped with a screen to isolate glow discharges, and is to have a remote-control unit which incorporates protective circuitry and a metal-sheathed bakeout unit which serves as a shield against stray magnetic fields. No isolation valve is specified because these pumps have demonstrated great reliability: recommended service interval is 35,000 h at 1 x 10^{-6} torr (3500 h at 1 x 10^{-5} torr).

Eighteen sorption pumps (total 101 lb of sieve material) are equipped with gas access screens, heating bands, shut-off valves, and stainless-steel Dewars for staged operation and rapid cycling. The roughing manifolds have Bourdon and thermocouple gauges, back-to-air and pressure-relief valves, provision for connecting auxiliary roughing system and purging gases, plus an all-metal bakeable isolation valve. The UHV portion of these manifolds will be equipped for bakeout to 350°C.

Pressure bumps in curved sections are minimized by use of SLAC/SPEAR-type distributed-ion pumps (LBL Assembly Drawing 16K3516) which nest inside the quadrant tanks and use the alternating-gradient fringing fields. A perforated screen provides charged-particle isolation of pump activity from beam space and serves to retain the pumps against the inner vertical chamber wall. These pumps are assembled as eight identical units with a combined active length of approximately 21 m, and are expected to provide a capacity of 4000 liters-sec^{-1} for hydrogen and 12,000 liters-sec^{-1} for air, based on previous experience.[53]

Additional reduction of beam-induced pressure bumps can be achieved by high-temperature vacuum bakeout of chamber components prior to or during fabrication.[54] Operational techniques are being developed[55] which promise an order-of-magnitude reduction in gas desorption. Some of these involve the use of considerable quantities of inert gas. Both sorption and triode sputter-ion pumps are excellent for use with such gases,[56,57] but triode pumps tend to be unstable while pumping argon between 6 x 10^{-5} and 1 x 10^{-5} torr and to overheat at higher pressures; however, commercially available

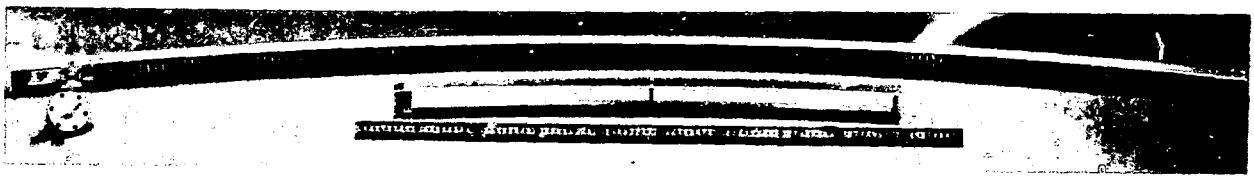

Fig. 19. Distributed-ion pump.

control units allow completely satisfactory operations. Additional inert gas capacity can be obtained by slotting the cathodes of the distributed ion pumps.[58,59]

High outgassing rate equipment (vertical extraction kicker, injection tube, extraction septum, rf cavity) has not been included in this proposal because designs for these items are not stabilized at this time. Each item presents a gas load which can be treated as a lump to be pumped locally. This approach permits earlier finalization of the remainder of the vacuum system. Therefore, this proposal assumes no gas flow across the boundaries of the above-mentioned equipment. A summary of the PSR vacuum parameters is given in Table V.

2. Operation.

Purging. Initial operation of the vacuum system can be preceded by a flushing process using carbon dioxide.[60] Heaters on the vacuum chamber can be cycled to above 100°C before and during purge to assist in removal of moisture to the atmosphere.

Roughing. Before rough pumping, the sorption pumps must be conditioned by warming them to ambient temperature. Warm-up with wraparound heaters, requires 30 min (stainless-steel Dewars need not be removed). A conservative roughing time is about 20 min.

First-Stage High-Vacuum Pumping. The commercial noble sputter-ion pumps can be started at pressures as high as 1 x 10^{-2} torr; operation is completely automatic by use of a pressure-sensitive relay in conjunction with a properly selected control unit, which provides log pressure, voltage, and current information. After about 4 h of evacuation, a 24-h 300-to 350°C baking cycle begins. Application of heater power must be monitored to avoid excessive initial pressure rise.

Final Stage UHV Pumping. When the vacuum system has cooled to near-ambient temperature and

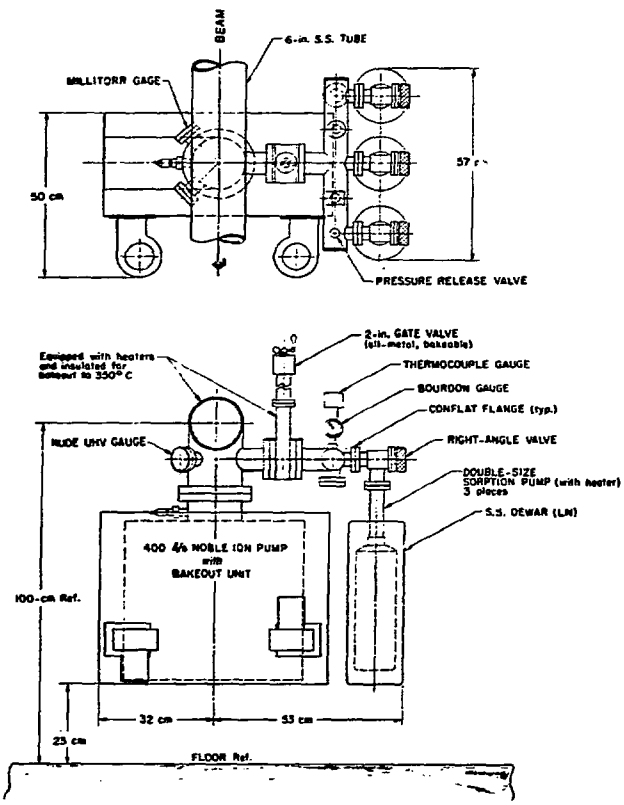

Fig. 20. Vacuum pumping station.

pressure at the 45° station in the bending section (quadrant) vacuum tanks has been reduced to 10^{-7} torr (approximately 5 h after end of bake), the distributed-ion pumps can be started. If isolation valves in the short straight sections are closed, one distributed-ion pump in each of two quadrant tanks is remote from an active pump. Start-up of these remote pumps will be delayed until a specified pressure is attained throughout the quadrant tank by operation of its neighbor pump.

TABLE V

SUMMARY OF VACUUM SYSTEM

Item	Area (m^2)	Volume (liters)
Curved quadrant tanks (4 only, at 3.16 m^2 each)	12.6	303
6-in.-o.d. straight tubes	15.2	528
UHV pump stations (6 only, at 0.14 m^2 each)	0.8	100[a]
Distributed ion pumps (8 only, at 4.09 m^2 each)	32.7[b]	-
Perforated screens (4 only, at 0.82 m^2 each)	3.3	-
Totals	64.6	931

[a]Includes internal volume of triode pumps.
[b]Area of equivalent stainless steel.

3. Performance.

Roughing. The system is expected to follow closely the pump-down schedule indicated in Varian Associates VacSorb information leaflet VAC 2292C for multiple stages, which calls for 10^{-3} torr in approximately 10 to 15 min; this agrees closely with F. Reinath in his calculation of June 27, 1971.[61] The WNRF system has more sorption material per unit volume than either, and thus is conservative.

High-Vacuum Region. If we extrapolate the data listed by Strausser[62] for degreased stainless steel (outgassing rate q in torr-liter-sec^{-1}-cm^{-2} equals 2×10^{-9} at 1 h, 1×10^{-9} at 2 h, 2.5×10^{-10} at 10 h, 8×10^{-11} at 40 h prior to baking), we obtain average pressures for the external sputter-ion pumps of 6×10^{-7}, 3×10^{-7}, 7×10^{-8}, and 2×10^{-8} torr at respective times without bakeout. Following a 24-h bakeout at 350°C, the average external pump pressure will approach the ultimate of 1×10^{-9} torr without internal ion pumping. Average pressure around the ring will be about 4×10^{-9} torr. With all pumps operating, the average ultimate pressure at pumps will be near 3×10^{-10} torr; average pressure around the ring will be slightly higher, 5×10^{-10} torr. This pressure will be attained after 2½ to 3 days of pumping.

III. THEORETICAL ANALYSES OF POSSIBLE ELECTROMAGNETIC EFFECTS IN PSR

This section is a theoretical survey of coherent electromagnetic effects pertaining to the WNRF PSR. The effects of the electromagnetic self-forces of the beam on both the inherent and coherent motion of beam particles are evaluated. The calculations are based, for the most part, on existing theory. In some instances, experimental observations in operating accelerator and storage rings are cited. For the design parameters of the ring, calculations indicate that only the transverse coherent instability may be troublesome, but may be suppressed by feedback. The design parameters of the ring that are pertinent to this work appear in Table VI.

TABLE VI

GLOSSARY OF SYMBOLS USED IN DISCUSSION OF ELECTROMAGNETIC EFFECTS IN PSR

Symbol	Meaning	Value
a	semimajor axis of elliptical beam	5 cm
b	semiminor axis of elliptical beam	1 cm
B	fraction of ring circumference occupied by protons	
B_{dc}	dc component of beam's magnetic self-field	
c	speed of light	3×10^{10} cm/sec
e	proton charge	4.8×10^{-10} esu
D	total width of rectangular vacuum tank	16 cm
E	total relativistic energy of protons	1.735 GeV
E_θ	azimuthal electric self-field	
f	circulation frequency	4 MHz
g	distance from orbit to magnetic surface	6 cm
g_o	geometric factor in expression for E_θ	
G	separation of two infinite conducting planes	
h	harmonic number	50
H	semiminor axis of elliptical vacuum tank	4 cm
m_o	rest mass of proton	
n	fractional neutralization of the beam	
N	total number of protons circulating in the ring	
	high-current mode	5.3×10^{13}
	pulse mode	5×10^{11}
N_b	number of protons in one rf bucket	10^{11}
r_b	radius of a beam with circular cross section	2 cm
r_c	radius of vacuum pipe with circular cross section	7.72 cm (3 in.)
r_p	classical proton radius	1.536×10^{-16} cm
R	average radius of ring	10^3 cm
T	total height of rectangular vacuum tank	8 cm
V	peak voltage on the rf cavity	
V_o	effective peak voltage including longitudinal space charge	
W	semimajor axis of elliptical vacuum tank	8 cm
Z_s	shunt impedance of the rf cavity	
Z_o	impedance of free space	377 Ω
β	particle speed in units of light speed	0.842
γ	particle energy in units of rest energy	1.85
γ_t	transition energy of ring	5.4
Δ	parameter characterizing width of flat beam	
ΔE	total energy spread in the beam	1.42×10^{-3} E
ϵ_1, ϵ_2	geometric factors	
η	$\gamma^{-2} - \gamma_t^{-2}$	0.2
θ	azimuthal coordinate	
λ	charge per unit length in beam	
ν_x	radial betatron wave number in external field	4.364
ν_y	vertical betatron wave number in external field	2.343
ν_s	vertical betatron wave number in presence of self-forces	
ω	angular frequency of perturbations	
ω_o	angular circulation frequency = 2πf	$8\pi \times 10^6$ sec^{-1}
ϕ	rf phase angle = h(θ-ω_ot) + π	
σ	conductivity of the vacuum-tank walls	10^{16} sec^{-1}
τ_g	exponential growth time of an instability	

A. Transverse Space-Charge Effects

The coherent self-electromagnetic fields of the beam exert forces on individual particles in the beam and alter their transverse motion. This phenomenon is traditionally discussed in terms of a tune shift, i.e., change in the betatron wave number. In general, the influence of the image charges and currents in the beam's surroundings must be included in the treatment of the self-forces. As we shall see below, these image charges and currents play only a small role in determining the tune shifts for the PSR. We treat only the shift in vertical tune (the shift in radial tune is generally much smaller).

The mathematical model used here is that of a beam with uniform density and elliptical cross section with semimajor axis a and semiminor axis b. The vacuum tank is also assumed to be elliptical, with semiaxes W and H. This is an approximation to the actual vacuum tank in the curved sections of the ring. In the straight sections, the vacuum tank has a circular cross section, and can be treated as the limit W/H = 1. This model has been exhaustively treated by Laslett.[63] For our purposes, we can use the relation

$$\nu_y^2 - \nu_s^2 = 2r_p \, NRF/B\pi\beta^2\gamma^3 b \, (a+b) \quad . \qquad (1)$$

All quantities except F are defined in Table VI.

The quantity F in Eq. (1) embodies the effect of the surroundings as well as the charge neutralization, and can be expressed in the form

$$F = 1 - n\gamma^2 + \frac{b(a+b)}{H^2}\left[\varepsilon_1(1-n\gamma^2+B\beta^2\gamma^2)+\varepsilon_2 B(\beta\gamma H/g)^2\right] . \qquad (2)$$

In Eq. (2), n is the fractional charge neutralization and ε_1 is a function of H/W. The work of Ref. 63 considers the direct-current component of the beam's magnetic field, B_{dc}, to have diffused through the vacuum tank and to be normal to magnetic surfaces located a distance g above and below the beam centroid. For this model of the magnets, $\varepsilon_2 = \pi^2/24$. For storage times presently contemplated in PSR, it is doubtful that penetration will occur, but rather that all the beam's magnetic field will be contained within the vacuum tank. This configuration of magnetic field can be treated by setting ε_2/g^2 equal to $-\varepsilon_1/H^2$ in Eq. (2). We shall give numerical results for both field configurations.

Using the values a = 3 cm, b = 1 cm, H = 4 cm, W = 8 cm, and the numerical values in Table VI, we find from Eq. (1)

$$\nu_y^2 - \nu_s^2 = 5.43 \times 10^{-5} \, (NF/B) \quad . \qquad (3)$$

We first examine the pulse mode of operation. In this mode, it is unlikely that any neutralizing background will be present, so we set n = 0 in Eq. (2). Setting B = 0.1 and using the values g = 6 cm and $\varepsilon_1 = 0.172$ (for W/H = 2) we find F = 1.064 if B_{dc} has penetrated the vacuum tank and F = 1.043 if B_{dc} has not penetrated. In the round pipe $\varepsilon_1 = 0$, and we set $g = \infty$ in Eq. (2), since there is no magnetic surface present. Thus, F is unity in the absence of a neutralizing background.

From these results it is clear that the surroundings have a negligible effect on the tune shift in the pulse mode. With $N = 5 \times 10^{11}$ and B = 0.1, we find from Eq. (3)

$$\nu_y^2 - \nu_s^2 = 0.025 \quad , \qquad (4)$$

and a resulting shift in ν_y that is too small to be taken seriously.

In the high-current mode of operation, the beam is uniform in azimuth, thus B = 1. If B_{dc} has penetrated the tank walls, we find F = 1.26 - 3.58 n, and if B_{dc} does not penetrate, F = 1.043 (1 - 3.43 n). At pressures of the order of 10^{-9} torr, n reaches a value of unity in a time of the order of 1 sec. Thus, for storage times of the order of milliseconds, we can set n = 0. We have, in fact, included neutralization in this treatment only to provide a complete formula. Also, for such short storage times we can neglect penetration of B_{dc}, so that again F is very near unity. If an entire macropulse from LAMPF is stored in the ring, $N = 5.3 \times 10^{13}$, and Eq. (3) yields

$$\nu_y^2 - \nu_s^2 = 0.29 \quad , \qquad (5)$$

and the resulting tune shift is -0.06, again innocuous.

We now ask what value of N will result in a shift of ν_y to a resonance. Rather than considering an integral resonance, we consider the $\nu_x = 2\,\nu_y$ coupling resonance, and allow a tune shift of 0.2. As the time required to accumulate many macropulses in the ring is many milliseconds, we allow for penetration of B_{dc}. To take the most pessimistic situation, we use n = 0, thus F = 1.26. We find that

$\Delta\nu_y = -0.2$ if $N = 1.3 \times 10^{14}$--a circulating current of 86 A. For F = 1, we find a current of 108 A.

The work of Ref. 63 also includes the effect of image charges and currents on the coherent transverse motion of the beam. This effect is less troublesome at low energy than is the incoherent tune shift treated above. It appears to be negligible for the PSR.

B. Longitudinal Space-Charge Effect

Since the ring will operate below the transition energy, the longitudinal electromagnetic self-force of the bunch will tend to cancel the bunching effect of the 201-MHz rf cavity. We wish to calculate the peak cavity voltage V necessary to accommodate a given energy spread in the presence of the self-force. It is not known how particles will be distributed in the stable phase area (bucket), but for the purposes of this calculation we assume a distribution that yields a charge per unit length λ given by

$$\lambda(\phi) = \lambda_o(1 - \cos\phi) \quad , \tag{6}$$

in which λ_o is a constant and $\phi = h(\theta - \omega_o t) + \pi$. In terms of the total number of particles in the bucket N_b, we have

$$\lambda_o = eh\, N_b/2\pi R \quad . \tag{7}$$

The energy change per turn from the cavity is $eV \sin\phi$, and the energy change from the azimuthal electric self-field E_θ is $2\pi eRE_\theta$, with E_θ given by

$$E_\theta = -\frac{g_o}{\gamma^2 R}\frac{d\lambda}{d\theta} = -\frac{g_o h}{\gamma^2 R}\frac{\partial\lambda}{d\phi} \quad . \tag{8}$$

In this expression, the quantity g_o is a geometric constant equal to $1 + 2\,\ell n\,(r_t/r_b)$ for a round beam in a round pipe. For a round beam between two infinite conducting planes separated by a distance G:

$$g_o = 1 + \ell n\,(2G/\pi r_b) \quad .$$

It is sufficient to take an average value of g around the ring in the following treatment. We thus have the energy change per turn $\delta E = eV_e \sin\phi$, in which the net voltage V_e is given by

$$V_e = V - (eh^2\, N_b\, g_o/\gamma^2 R) \quad . \tag{9}$$

From the numbers in Table VI, we find that g_o/γ^2 is near unity in the round pipe and slightly less if we calculate it using the expression for infinite plates and G = 2H. We take $g_o/\gamma^2 = 1$ and find

$$eh^2\, N_b\, g_o/\gamma^2\, R = 36\ \text{kV} \quad . \tag{10}$$

A peak voltage of 36 kV on the cavity is necessary to compensate for the self-field in the absence of energy spread.

The energy spread ΔE is related to the effective voltage V_e by the expression[64]

$$\frac{\Delta E}{E} = 2\beta\left(\frac{2eV_e}{\pi h\eta E}\right)^{\frac{1}{2}} \quad . \tag{11}$$

For a momentum spread $\Delta p/p = 2 \times 10^{-3}$, $\Delta E/E = 1.42 \times 10^{-3}$, and we find $V_e = 19.3$ kV. Although this calculation is based on a particular distribution of particles in the bucket, any reasonably smooth distribution will give similar results, and we conclude that a peak voltage of 60 kV on the buncher cavity should be sufficient to overcome the self-forces and accommodate the anticipated energy spread.

C. Coherent Instabilities

The electromagnetic self-fields of a beam of particles can react back on the particles in the beam and may cause the coherent motion of the beam particles to become unstable. The geometry and electromagnetic properties of the beam's surroundings play an important role in this phenomenon. For a beam that is uniform in azimuth, a theoretical analysis exists for most such instabilities, and the theory is rather well established. The theory is not so well understood for unstable motion in bunched beams. However, certain instabilities that have been observed in bunched beams have been successfully suppressed by methods applicable to the PSR.

The situation with regard to instabilities in this device is in some ways more severe than in existing machines because of the relatively high current (in the high-current mode), the very small energy spread, and the relatively low energy. On the other hand, the device has the advantage of operating below the transition energy, thus eliminating the negative mass instability.[65] Additional advantages are a large aperture, very good vacuum, and short storage times. We discuss several of the known instabilities, predict which of these may be troublesome in this device, and suggest the methods that may be used to suppress them.

1. Longitudinal Resistive Wall Instability.[66]

This instability, a distant cousin of the negative mass instability, arises from the finite conductivity of the vacuum tank and leads to longitudinal bunching of an azimuthally uniform beam. For a beam

with no spread in circulation frequency, we first estimate the growth rate of this instability in the simplest possible geometry. We take a beam with circular cross section and uniform density out to radius $r = r_b$ inside a pipe of circular cross section and radius r_t. The growth time τ_g is found from Eq. (4.6) of Ref. 66,

$$\tau_g = \frac{r_t}{\beta\gamma R}\left[\frac{1 + 2\,\ell n\,(r_t/r_b)}{2\pi R\, Ne^2\, f\,(df/dE)}\right]^{\frac{1}{2}} , \qquad (12)$$

in which $R = (\omega/8\pi\sigma)^{\frac{1}{2}}$, with σ the conductivity of the wall material and ω the angular frequency of the longitudinal oscillations ($\omega = 2\pi\ell f$, with ℓ an integer). We further have

$$\frac{df}{dE} = \frac{f^2}{\beta^2 E}\left(\frac{1}{\gamma^2} - \frac{1}{\gamma_t^2}\right) , \qquad (13)$$

with f the particle's circulation frequency and E the total particle energy. We take $r_b = 2$ cm, $r_t = 7.72$ cm (3 in.), and $\sigma = 10^{16}$ sec^{-1}--typical of stainless steel. For $N = 5.3 \times 10^{13}$, we find $\tau_g = 0.083/\ell^{\frac{1}{2}}$ sec. This time is sufficiently long that the instability should not be a problem in the ring. More elaborate expressions for the growth time can be employed, but do not give results that alter this conclusion.

2. Transverse Resistive Wall Instability.

This instability, which also arises from the finite conductivity of the vacuum tank, can cause unstable coherent transverse motion of the beam. We first calculate the growth rate using the same model as used above. Again, we are considering the high-current mode of PSR operation ($N = 5.3 \times 10^{13}$). The growth time is given by Eqs. (1.17b) and (4.4) of Ref. 67.

$$\tau_g = \pi\nu_y\, \gamma m_o\, \omega r_t^3/e^2\, N\beta R \quad . \qquad (14)$$

The allowed values of ω for this instability are $2\pi(\ell - \nu_y)f$, with ℓ an integer greater than ν_y. The shortest growth time occurs for $\ell = 3$, for which we find $\omega = 1.52 \times 10^7$ sec^{-1} and $R = 7.75 \times 10^{-6}$. For the same numbers used above we find $\tau_g = 2$ msec.

The theory of Ref. 67 is also applicable to a ribbon beam in a vacuum tank with rectangular cross section of width D and height T. Employing Eq. (3.26b) of Ref. 67, we have

$$\tau_g = 3\,\nu_y\, \gamma m_o\, \omega\, T^3/2\pi e^2\, N\beta R\, F_3\,(T/D,\, \Delta/T) \quad . \qquad (15)$$

In this expression Δ characterizes the half-width of the beam and the function F_3 is presented in Fig. 5 of Ref. 67. To approximate the geometry of the vacuum tank in the bending magnets, we take T/D = 1/2 and $\Delta/T = 3/4$, and find $F_3 = 0.9$. For the usual numbers, and T = 8 cm, we find $\tau_g = 0.38$ msec.

If the growth time really is as long as 2 msec, it might be possible to beat this instability by filling the ring using a single LAMPF macropulse (17-mA H^-) and extracting the beam immediately. However, the value of $\tau_g = 0.38$ msec predicts that the instability may well occur, even if this option can be employed. The actual growth time should be somewhat between these two limits. At this low energy it is not practical to obtain the amount of betatron frequency spread necessary to suppress the instability by Landau damping. However, transverse instabilities have been suppressed by feedback in a number of circular machines, and this method is applicable to PSR.

The growth time for the $\ell = 4$ mode is 1.63 times τ_g for the $\ell = 3$ mode, so this mode as well as the $\ell = 5$ mode may become troublesome. The feedback mechanism should be sufficiently broad-band to stabilize the first few modes. A description of the feedback mechanism used in the Stanford electron-positron storage ring SPEAR can be found in Ref. 68.

3. Transverse Instability in a Bunched Beam.

The unstable coherent motion of a bunched beam has been treated by Courant and Sessler,[69] who consider the effect of the wake fields left in the vacuum tank on previous turns. Their work leads to selection rules for the ν values. These selection rules have been adhered to in the design of the ring.

The theory of Ref. 69 has not been successful, however, for interpreting experimental results. The effect of the local fields is considered in the so-called head-tail instability.[70] The theory of Ref. 70 predicts that if the chromaticity ($\partial\nu/\partial E$) is positive, the coherent motion is stabilized. This aspect of the theory has been verified by experiments with SPEAR.[71] The design of the PSR is such that $\partial\nu/\partial E$ can be tuned either positive or negative in either or both planes. Also, the SPEAR experiments demonstrated that the motion could be stabilized by means of feedback. Although the physical phenomena responsible for the instability are not fully understood, the results of the SPEAR experiments indicate

that should this occur in the PSR it could be suppressed.

4. Beam Cavity Interaction.[72] The 201.25-MHz cavity will be present in the ring during operation in the high-current mode, but it can easily be shorted. If the cavity is not shorted, and its shunt impedance is above a critical value, its presence can give rise to longitudinal bunching of the beam in the high-current mode. The upper limit on the shunt impedance Z_s can be found from Eq. (4.8) of Ref. 70, which may be written as

$$\frac{Z_s}{Z_o} < \frac{hc\,(\Delta E)^2\,\eta}{e^2 N\beta^2\, fE} \quad , \tag{16}$$

in which h is the harmonic number (= 50), Z_o is the impedance of free space (377 Ω), and ΔE is the full-energy spread in the beam. We find

$$\frac{Z_s}{Z_o} < 2.4 \times 10^{-7}\left(\frac{\Delta E}{E}\right)^2 \quad , \tag{17}$$

and for $\Delta E/E = \sqrt{2} \times 10^{-3}$ we have $Z_s < 48\, Z_o$ or 18 kΩ. This value should not place stringent requirements on the cavity design. If Z_s exceeds this value, the cavity can be shorted.

5. Beam-Background Instability. A transverse beam instability attributed to the interaction of the beam and the ionized background has been treated theoretically.[73,74] The instability has been observed in the Bevatron, where it was suppressed by inserting clearing electrodes to remove the background particles.[75] The background particles oscillate transversely in the potential well of the beam. When this frequency is near the frequency $(\ell - \nu)f$, a coherent motion of the background couples to a coherent transverse motion of the beam. No simple analytic formulas exist for the threshold or growth rate of the instability, so that results must be obtained computationally.

For PSR, a simple model was investigated to determine whether the instability would occur. The model consists of a beam inside a perfectly conducting pipe, both of circular cross section. The beam and background densities are uniform out to a radius $r = r_b$, and zero for $r > r_b$. Both species are assumed to move as rigid bodies. The beam is monoenergetic with no transverse particle motion, and the background temperature is zero. This model is not only simple, but should also give pessimistic results because all the damping mechanisms (e.g., background temperature, spread in particle energy and betatron frequency) have been left out.

The results show that for a circulating current of 100 A, no instability occurs for a fractional neutralization n = 0.1. As stated above, the pertinent frequencies are $\omega = (\ell - \nu)\,\omega_o$. For n = 0.5 (50% neutralization) all modes such that $65 < \ell < 71$ are unstable. At the background pressure of 10^{-9} torr, a value of n = 0.1 will not be attained in the short storage time of the high-current mode. Thus, one feels reasonably certain that this instability will not be a problem in the ring.

There is a troublesome phenomenon in the CERN proton storage rings that has been attributed to local regions of enhanced background density. The effect is being investigated, and may well be pertinent to PSR in that the stripping foil may produce such a region of relatively high background density. It should be pointed out, however, that this is not a major concern; indeed, the CERN rings operate quite successfully.

IV. INSTRUMENTATION

A. Beam Observation and Control

As storage rings become more complex, lattice manipulations involve complicated interrelations between magnet currents and are much too complex to be handled manually in any reasonable time. The control of magnets as well as most other monitoring and control elements in SPEAR is accomplished by computer. The SPEAR system allows the operator to choose any values of tunes, betas, and dispersions and to vary any subset of these parameters while holding the other constant.[76] This computerized control system has been responsible for the determination of beam instabilities and for the fact that the design luminosity for SPEAR was attained within 3 days of initial operation.

The magnet system for PSR, because of its structure, will suffer from parameter interaction difficulties. It is presently anticipated that the only major instability in the PSR can be controlled through inverse passive feedback. However, small computer memory cycle times are now approaching durations useful to the PSR as active computer feedback systems. Successful operation of the PSR, whether feedback is human-controlled or computer-controlled, will depend on accurate sensing of all

PSR functions. Accurate sensing of H^- beam input, stripping, and proton beam accumulation as well as extraction must be maintained and analyzed if the system is to serve as a test vehicle for attainment of ultrahigh currents.

In particular, it is necessary to know whether the beam is striking the stripper foil in the correct position to place the protons on the PSR equilibrium orbit; it is necessary to know whether this equilibrium orbit is properly adjusted for the proton momentum; it is necessary to know what individual particle motion and what collective motion about the equilibrium orbit is occurring; and it is necessary to know whether the extraction system is removing the particles from the proper portion of the beam without disturbing the remainder.

It is worth noting, briefly, how much information about the beam is required (i.e., how little is sufficient), since obviously the complete distribution function presenting beam density and motion for all coordinates and time is neither obtainable nor necessary. One notes that in the understanding of subtle instabilities that will undoubtedly arise with ultrahigh currents, the craftsman is indeed limited by his tools--a very much greater precision and number of measurements will have to be made.

1. To carry out injecting, stripping, and loading at low particle density, we need to have an acceptable equilibrium orbit and acceptably small transverse oscillations about this orbit. Adjustable parameters are input steering magnets, and ring bending and focusing magnets. For guiding these measurements and attaining a suitable equilibrium orbit, it is sufficient to know the position of the center of mass of the beam at the stripping foil, and at a number of stations around the PSR. If it can be assumed that the center-of-mass orbit and divergence of the input beam are reproducible, only the time-average beam position at the selected positions is needed.

1. At high current density, when collective behavior becomes important, we need to know center-of-mass motion resolved to the time scale of the characteristic collective frequencies. We need also the longitudinal distribution and the beam cross section (i.e., the energy spread and transverse amplitude distribution) since beam collective stability is controlled by particle distribution in energy and transverse amplitude. In the past, most instabilities have been manifested as growth of collective center-of-mass oscillation, but as we now move into a current regime not previously attained, the possibility exists of higher order modes. We therefore need to be prepared to obtain the more detailed information about the distribution in beam transverse coordinates required to deal with such modes. Specifically, we need to be prepared to observe at least the third and fourth moments of the transverse distribution (the first and second moments correspond to center-of-mass displacement and rms beam size).

3. Feedback control of instabilities depends on sensing elements responsive to whatever collective modes are to be suppressed and, thus the sensing requirements are the same as for observation of the modes. We plan initially to use passive feedback to stabilize only the lowest order center-of-mass displacing mode. Problems involving higher modes will be confronted when or if they arise.

B. Observational Equipment

Sources of information about the beam will include:

1. Glow From the Stripper Foil. With injection and stripping by a carbon foil visual observation will provide useful information about the average position of the beam which should facilitate adjustment of the input optics to the PSR.

2. Adjustable Beam Targets. Other foils, wires, or flags introduced around the PSR will provide additional beam-position information. For the lowest beam intensity, a fluorescent screen will give the most sensitive indication of location and distribution, while at higher currents foils heated to incandescence may prove useful. For pulse-mode operation, electromagnetic coupling should be sufficient to use inductive loop sensing.

3. Rogowski Coil. For measurements of total accumulated circulating current in the high-current mode, a Rogowski coil encircling the beam inside the vacuum chamber will be useful. (On the time scale of interest, magnetic field effects outside the vacuum chamber will not be usable for current measurement as they are in SPEAR and at the CERN ISR.)

4. Pickup Plates and Loops. The simplest system for detection of beam position within the vacuum chamber is an array of four electrostatic

pickup plates at the top, bottom, and sides of the chamber. An alternative is to use magnetic pick-up loops. Both methods can be calibrated to give an indication of the total current, thus supplementing the Rogowski observations.

5. Strip Lines Coupled to Beam. Previous work has shown that 50-Ω strip lines of 30 cm or more length, inside the vacuum chamber, can provide coupling to the beam suitable for determination of position and for applying necessary inverse feedback for control of collective oscillations. Such lines are found to be fairly flat in frequency response, which is a desirable feature for simultaneous detection of several collective modes with the same transducer.

6. Fast-Framing, Phased-Array PSR Beam Profile Monitor. An extremely versatile, rugged, and radiation-resistant fast-framing camera has been developed by LASL for weapons field testing. This camera has many unique properties which, when coupled with a beam-profile monitoring device such as the CERN beam detector, will make it possible to study profiles of even portions of PSR micropulses.[77] The camera consists of eight or more frames with shutter durations down to 1 nsec (although the system is typically limited by the speed of the fluor, which in this case is 2.7 nsec for plastic--for higher speeds radiachromics must be used).[78-80]

The system is based upon the phased-array concept of triggering, using a common trigger pulse and distributing it to each shutter via passive delay cables.[81] This makes it ideal for taking frames in phase from stations located around the PSR. Such a system provides variable interframe times and zero interframe jitter. Simple intensifier diodes could be used, or, for situations demanding the least amount of target material in the beam, the high-gain Generation II planar intensifier could be employed.[77,78]

Such a television system, when coupled to a gas curtain target (see Fig. 21) offers framing times to 2.7 nsec (one-half a pulse) which would be very useful in studying head-tail instabilities with a minimum of scattering material in the beam. The CERN method of collection of stripped electrons by postacceleration provides an ultrahigh-speed transducer. Channel plates or Johnston multiplier arrays

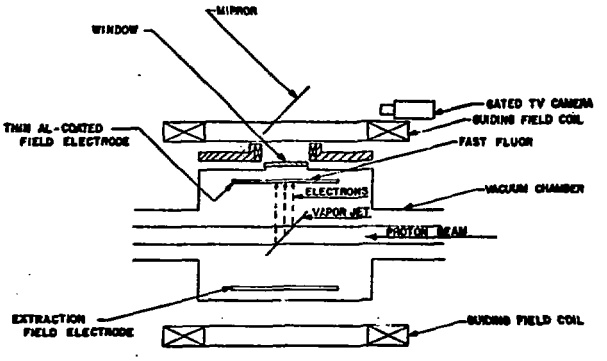

Fig. 21. Beam profile transducer.

could be used to yield gain. It should be emphasized that the television system offers the most reliable means of "pictel" commutation, and, therefore, visual display. Employment of sophisticated intensifiers may be warranted even though the detail required is low, for their gain reduces target perturbation on the beam. In fact, for integrated exposure, residual gas may provide enough electrons for imaging.

7. Radio-Frequency Excitation. The precise measurement of transverse oscillation frequencies will be made by observing the resonant response of the beam to applied transverse rf fields. This method gives single-particle frequencies at low beam intensities by observation of resonant growth of beam center-of-mass motion. Change of particle amplitude distribution within the beam arises from selective amplitude growth of the fractional population of particles in resonance with the applied field at a given excitation frequency.

C. Hardware Required

For observational access to the beam, the vacuum chamber will be provided with a large number of standard copper-gasketed ports, mostly in groups of four located on the top, bottom, and sides of a given azimuth. Such ports allow for installation of any type of observational device that may be required, and permit easy modification when necessary. The estimated installed cost per port is of the order of $300 for a 1.3-in. clear opening and $600 for a 3-in. clear opening. Thus, where a high concentration of electrical connections is required, as for a feedback section requiring four strip line

sensors and four strip line drivers with two connections per strip line, it may be preferable to build a special piece of straight section with the components permanently installed. (This is the choice made at SPEAR.) Also, for the electron acceleration and gas curtain systems, either a special installation or unusually large ports will be required. In addition to the vacuum chamber access, the observations will call for a variety of standard and special equipment. This need will be developed as attainment of PSR goals is met.

REFERENCES

1. D. W. Kerst, F. T. Cole, H. R. Crane, L. W. Jones, L. J. Laslett, T. Ohkawa, A. M. Sessler, K. R. Symon, K. M. Terwilliger, and N. Vogt Nilsen, "Attainment of Very High Energy by Means of Interacting Beams of Particles," Phys. Rev. 102, 590 (1956).

2. William M. Brobeck, "Design of High Energy Accelerators," Symposium on High Energy Accelerators, CERN, 1956, p. 60.

3. G. K. O'Neill, "Storage Ring Synchrotron Device for High Energy Particle Research," Phys. Rev. 102, 1418 (1956).

4. CERN Study Group in New Accelerators, "The Design Study of Intersecting Storage Ring (ISR) for the CERN Proton Synchrotron," CERN Laboratory report AR/Int. SG/64-9 (1964).

5. Burton Riechter, "Initial Operating Results from SPEAR," Invited Paper, 1973 Particle Accelerator Conference, San Francisco, California, March 5-7, 1973, IEEE Trans. Nuc. Sci., Vol. NS-20, No. 3, 752-755.

6. A. N. Skrinsky, "Storage Ring Program at Novosibirsk," Ref. 5, pp. 756-759.

7. H. Funsten, A. Lieber, R. Roberson, and R. Sherr, "Duty-Factor Improvement in the Princeton FM Cyclotron," Bull. Am. Phys. Soc. Series II, 8, 13 (1963).

8. H. Funsten, R. Roberson, A. Lieber, and R. Scherr, "Effects of Stochastic Acceleration on Beam Structure in the Princeton FM Cyclotron," Rev. Sci. Instr. 35, 1653-1657 (1964).

9. R. G. Fluharty, personal communication.

10. R. R. Fullwood, Compiler, "Design Study for a Medium-Energy, Intense, Proton-Storage Ring (WNR Ring)," Los Alamos Scientific Laboratory report LA-4946 (July 1972).

11. J. D. Simpson, "Operating Results from ANL Booster," Ref. 5, pp. 198-201.

12. Henri Bruck, "Accelerateurs Circulaires de Particules," Institut National des Science et Techniques Nucleaires, Saclay, 1966.

13. J. E. Osher, F. J. Gordon, and G. W. Hamilton, "Production of Intense Negative Hydrogen Beams," Proc. 2nd Intern. Conf. Ion Sources, Vienna, 1972, p. 876.

14. G. P. Lawrence, A. R. Koelle, J. L. McKibben, T. B. Clegg, and G. Roy, Ref. 13, p. 505.

15. K. L. Brown and S. K. Howry, "Transport 360 G Computer Program for Designing Charged Particle Beam Transport Systems," Stanford Linear Accelerator report SLAC-91 (1970).

16. "WNR Storage Ring Stripper Experiment," LAMPF Machine Research Proposal 128, A. Lieber, Spokesman, Los Alamos Scientific Laboratory internal document, August 1972.

17. E. D. Courant and H. S. Snyder, "Theory of the Alternating Gradient Synchrotron," Ann. Phys. 3, 23 (1958).

18. P. F. Meads, Jr., "An 'Invisible' Long Straight Section for Synchrotrons," Nucl. Inst. & Methods 96, 351-354 (1971).

19. J. Gunn, Lawrence Berkeley Laboratory, personal communication, January 1972.

20. P. F. Meads, Jr., "Parameter Study of the 'Invisible' Long Straight Section for Synchrotrons," Ref. 5, pp. 875-876.

21. J. Gunn, Lawrence Berkeley Laboratory, personal communication with A. J. Lieber, March 1973.

22. Ref. 12, Chap. 10.

23. A. Schoch, "Theory of Linear and Nonlinear Perturbations of Betatron Oscillations in Alternating Gradient Synchrotrons," CERN 57-21 (1958).

24. J. Laslett, "On Harmonic Response of Closed Orbit Alternating Gradient Synchrotron," Lawrence Berkeley Laboratory report UCID-10157 (June 4, 1965).

25. J. Laslett, "Computational Results Concerning Maximum Displacement of a Closed Orbit for One and Two Transverse Degrees of Freedom," Lawrence Berkeley Laboratory report UCID-10158 (May 1965).

26. J. Laslett and J. E. Braley, "On the Relative Weights of Cords and Perpendicular Measurements in Determining the Radial Position of Primary Survey Monuments for an Alternating Gradient Synchrotron," Lawrence Berkeley Laboratory report UCID-10160 (August 15, 1966).

27. J. Laslett and L. Smith, "Analysis of Surveying Procedures that Only Employ Distance Measurements and the Effects of Surveying Errors on the Closed Orbit," Lawrence Berkeley Laboratory report UCID-10161 (May 1965).

28. L. Smith, "Effects of Errors and Correcting Elements on Betatron Oscillations," Lawrence Berkeley Laboratory report UCID-1420 (January 1961).

29. Ref. 27, p. 3ff.

30. "200 BeV Accelerator Design Study," Vol. I, Chapter IV, Lawrence Berkeley Laboratory report (June 1965).

31. Ref. 10, pp. 16-17.

32. P. F. Meads, Jr., "New Methods for Multiturn Injection into Synchrotrons," Ref. 5, pp. 401-402.

33. Ref. 13, p. 877.

34. I. I. Bel'chenko, G. I. Dimov, and V. G. Dudnikov, "Production of an Intense H^- Ion Beam from a Discharge in Crossed Fields," IIF an SSSR Sibirskoe Otdelenie, Preprint IIF 66-72, Translated, Los Alamos Scientific Laboratory report LA-TR-73-1.

35. G. I. Dimov and G. V. Rosliakov, "An Investigation of a Pulsed Charge-Exchange Source of Negative Hydrogen Ions," Preprint IIF 35-73, Novosibirsk (1973), Translated, Los Alamos Scientific Laboratory report LA-TR-73-47.

36. T. J. M. Sluyters and K. Prelec, Nucl. Instr. & Methods (to be published).

37. K. Prelec and T. J. M. Sluyters, "Formation of Negative Hydrogen in Direct Extraction Sources," submitted to Rev. Sci. Instr., June 1973.

38. T. J. M. Sluyters, Brookhaven National Laboratory, personal communication with T. D. Hayward, July 25, 1973.

39. W. Gruebler, P. A. Schmelzbach, V. König, and P. Marmier, Helv. Phys. Acta 43, 254 (1969).

40. Ref. 10, p. 11.

41. G. M. Stinson, W. C. Olsen, W. J. McDonald, P. Ford, D. Axen, and E. W. Blackmore, "Electric Dissociation of H^- Ions by Magnetic Fields," Nucl. Instr. & Methods 74, 333 (1969).

42. H. C. Bryant, P. A. Lovoi, G. G. Ohlsen, "Production of Pulsed Particle Beams by Photodetachment of H^-," Phys. Rev. Lett. 27, 24 (December 13, 1971).

43. A. J. Gorka, "A Fast Spinning Stripper Mod II for the Zero Gradient Synchrotron (ZGS) Booster," Ref. 5, pp. 387-391.

44. N. Laulainen and H. Bichsel, "Energy Removed by Delta Rays from Finite Volumes in Passage of Charged Particles," Nucl. Instr. & Methods 104, 531-539 (1972).

45. Ref. 10, p. 15.

46. G. S. Brady, Materials Handbook, 10th Edition, 1971, p. 376.

47. J. E. Brolley, "Density Profiles of a Supersonic Jet Target," Ref. 5, pp. 475-477.

48. A. B. Tucker and A. J. Lieber, "Directional Neutron Spectrometer," IEEE Trans. Nucl. Sci., 13th Symp. on Nucl. Sci. Inst. in Space & Lab, Boston, Mass., October 20, 1966.

49. R. T. Avery, Lawrence Berkeley Laboratory, personal communications with A. Lieber, May and July 1972.

50. R. T. Avery, "Kicker Septum Conceptual Design 'D'," Lawrence Berkeley Laboratory report UCID-3570 (May 12, 1972).

51. R. T. Avery, "Septum Mag 'ES-1' Design D," Lawrence Berkeley Laboratory report UCID-3567 (April 10, 1972).

52. W. Schnell, "Operating Results from ISR," in Ref. 5.

53. V. Cummings et al., "Vacuum System for Stanford Storage Ring, SPEAR," J. Vac. Sci. & Tech. 8, 348 (1971).

54. R. Calder et al., "Reduction of Stainless Steel Outgassing in Ultra-High Vacuum," CERN-ISR-VAC/66-28 (September 23, 1966).

55. R. Calder, "The Vacuum System of the ISR," CERN Courier, No. 11, Vol. 12 (November 1972).

56. Varian Associates, VAC 2227D.

57. Varian Associates, VAC 2292C.

58. V. E. Hoffman, "Ion Pumping," Industrial Research (September 1964).

59. R. L. Jepsen et al., Trans. 7th A. V. S. Nat'l Symp., Pergamon Press, Oxford, 1961.

60. A. H. Beck, Handbook of Vacuum Physics, Vol. I, Parts 1-3 (1964) p. 123.

61. F. Reinath, Lawrence Berkeley Laboratory, personal communication with D. Norgren, June 27, 1971.

62. Y. Strausser, "Review of Outgassing Results," Varian Associates, Vacuum Division report VR-51, Table 10.

63. L. J. Laslett, "On Intensity Limitations Imposed by Transverse Space-Charge Effects in Circular Particle Accelerators," Proc. 1963 Summer Study on Storage Rings, etc., Brookhaven National Laboratory report BNL-7534, p. 324 (1963).

64. C. Bovet et al., "A Selection of Formulae and Data Useful for the Design of A. G. Synchrotrons," CERN/MPS-SI/Int. DL/70/4, p. 31 (1970).

65. C. E. Nielsen, A. M. Sessler, and K. R. Symon, Proc. Intern. Conf. High Energy Accelerators, CERN, Geneva, 1959, p. 239.

66. V. K. Neil and A. M. Sessler, "Longitudinal Resistive Instabilities of Intense Coasting Beams in Particle Accelerators," Rev. Sci. Instr. 36, 429-436 (1965).

67. L. J. Laslett, V. K. Neil, and A. M. Sessler, Ref. 65, p. 436.

68. J. Pellegrin, "Beam Feedback Electronics for the SPEAR Storage Ring," Stanford Linear Accelerator Center report SLAC-Pub-1150 (1972).

69. E. D. Courant and A. M. Sessler, "Transverse Coherent Resistive Instabilities of Azimuthally Bunched Beams in Particle Accelerators," Rev. Sci. Instr. 37, 1579-1588 (1966).

70. C. Pellegrini, "On a New Instability in Electron-Positron Storage Rings (The Head-Tail Effect)," Nuovo Cimento 64A, 447-473 (1969).

71. The SPEAR Storage Ring Group, "Operating Results from SPEAR," Stanford Linear Accelerator Center report SLAC-Pub-1215. To appear in Proceedings of 1973 Particle Accelerator Conference, San Francisco, California, 1973.

72. L. J. Laslett, V. K. Neil, and A. M. Sessler, "Coherent Electromagnetic Effects in High Current Particle Accelerators: III. Electromagnetic Coupling Instabilities in a Coasting Beam," Rev. Sci. Instr. 32, 276-279 (1961).

73. D. G. Koshkarev and P. R. Zenkevich, "Resonance of Coupled Transverse Oscillations in Two Beams," Particle Accelerators 3, 1-9 (1972).

74. L. J. Laslett, A. M. Sessler, and D. Mohl, "Transverse Two-Stream Instability in the Presence of Strong Species-Species and Image Forces," Lawrence Berkeley Laboratory report LBL-1072 (1972).

75. H. A. Grunder and G. R. Lambertson, "Transverse Beam Instabilities at the Bevatron," Proc. of the 8th Intern. Conf. on High Energy Accelerators, CERN, Geneva, 1971.

76. Ref. 5, pp. 752-753.

77. "Sodium Jet Beam Detector," CERN Courier 11, Vol. II (November 1971)

78. G. J. Berzins, Ki. S. Han, A. J. Lieber, and John S. McGurn, "Nanosecond Photography of Radiachromic Processes," to be presented at Electro-Optical Systems Conference, September 18-20, 1973, New York, NY.

79. A. J. Lieber and H. D. Sutphin, "Nanosecond High Resolution Framing Camera," Rev. Sci. Instr. 42, pp. 1663-1667 (1971).

80. H. D. Sutphin and A. J. Lieber, "Nanosecond Framing Cameras Using Proximity Focused Image Intensifiers," Applications of Optical Electronics in Instrumentation 6th Inst. Symp., Inst. Soc. America, April 24, 1972. Basic Material in LA-4937-MS, Los Alamos Scientific Laboratory report (April 1972).

81. A. J. Lieber, "Nanosecond Gating of Proximity Focused Channel-Plate Intensifiers," Rev. Sci. Instr. 43, 104-108 (1972).